# The Hippo kinase cascade regulates a contractile cell behavior and cell density in a close unicellular relative of animals

**Authors:**

Jonathan E Phillips, Duojia Pan*

**Affiliation:**

Department of Physiology, Howard Hughes Medical Institute, University of Texas Southwestern Medical Center, Dallas, Texas 75390, USA

* correspondence: duojia.pan@utsouthwestern.edu

**ABSTRACT**

The genomes of close unicellular relatives of animals encode orthologs of many genes that regulate animal development. However, little is known about the function of such genes in unicellular organisms or the evolutionary process by which these genes came to function in multicellular development. The Hippo pathway, which regulates cell proliferation and tissue size in animals, is present in some of the closest unicellular relatives of animals, including the amoeboid organism *Capsaspora owczarzaki*. We previously showed that the *Capsaspora* ortholog of the Hippo pathway nuclear effector Yorkie/YAP/TAZ (coYki) regulates actin dynamics and the three-dimensional morphology of *Capsaspora* cell aggregates, but is dispensable for cell proliferation control (Phillips et al., 2022). However, the function of upstream Hippo pathway components, and whether and how they regulate coYki in *Capsaspora*, remained unknown. Here, we analyze the function of the upstream Hippo pathway kinases coHpo and coWts in *Capsaspora* by generating mutant lines for each gene. Loss of either kinase results in increased nuclear localization of coYki, indicating an ancient, premetazoan origin of this Hippo pathway regulatory mechanism. Strikingly, we find that loss of either kinase causes a contractile cell behavior and increased density of cell packing within *Capsaspora* aggregates. We further show that this increased cell density is not due to differences in proliferation, but rather actomyosin-dependent changes in the multicellular architecture of aggregates. Given its well-established role in cell density-regulated proliferation in animals, the increased density of cell packing in *coHpo* and *coWts* mutants suggests a shared and possibly ancient and conserved function of the Hippo pathway in cell density control. Together, these results implicate cytoskeletal regulation but not proliferation as an ancestral function of the Hippo pathway kinase cascade and uncover a novel role for Hippo signaling in regulating cell density in a proliferation-independent manner.

## INTRODUCTION

Despite the increasing recognition that the last unicellular ancestor of animals possessed many genetic components that mediate development in modern animals (Ros-Rocher et al., 2021), little is known about the function of such developmental regulators in the unicellular ancestor, and the process of how such genes came to function in these roles over evolutionary time is poorly understood. One example of a developmental pathway that is now known to be conserved in close unicellular relatives of animals is the Hippo pathway, which regulates tissue size in animals (Pan, 2022). The Hippo pathway consists of a kinase cascade in which the kinase Hippo/MST phosphorylates the kinase Warts/LATS, which in turn phosphorylates the transcriptional coactivator Yorkie/YAP/TAZ, resulting in inactivation though cytoplasmic sequestration (Figure 1A, (Ma et al., 2019)). In the nucleus, Yorkie/YAP/TAZ forms a complex with the transcription factor Sd/TEAD, and this complex drives the expression of genes that promote proliferation and affect cell differentiation (Wu et al., 2008). The Hippo pathway thus serves to inhibit Yorkie/YAP/TAZ activity, and by this regulatory activity restricts tissue growth in development and homeostasis. In cultured cells, the Hippo pathway is regulated by cell density in a process called contact inhibition, whereby Hippo signaling is low in sparse culture to allow cell proliferation but activated in confluent culture to arrest proliferation (Zhao et al., 2007). Although the state of the cytoskeleton (Dupont et al., 2011) and epithelial cell architecture (Yang et al., 2015) are known to regulate Hippo signaling, and many additional upstream regulatory components have been identified (Deng et al., 2015; Hamaratoglu et al., 2006; Yu et al., 2010; Zheng et al., 2017), how exactly Hippo signaling is regulated to achieve appropriate tissue size during development or stop cell proliferation in confluent cultures remains incompletely understood. As Hippo pathway dysregulation underlies multiple human cancer types (Zanconato et al., 2016), a more complete understanding of Hippo pathway regulation could guide the development of novel cancer therapeutics.

Although once thought to be present only in animals, the Hippo pathway is now known to be present in some of the closest unicellular relatives of animals (Figure 1B, (Sebe-Pedros et al., 2012)). One such unicellular organism is *Capsaspora owczarzaki* from the clade Filasterea, the sister group to Choanozoa (a clade comprising animals and choanoflagellates) (Shalchian-Tabrizi et al., 2008). The *Capsaspora* genome encodes all components of the core Hippo pathway as well as some conserved upstream Hippo pathway regulators such as Kibra and NF2/Merlin (Sebe-Pedros et al., 2012). *Capsaspora* is a motile amoeboid organism with a 5-micron-diameter

cell body covered with F-actin-rich filopodia-like structures, and was initially identified as an apparent endosymbiont in the snail *B. glabrata (Stibbs et al., 1979)*. However, all other known filasterians are apparent free-living heterotrophs (Hehenberger et al., 2017; Patterson et al., 1993; Tong, 1997), and whether *Capsaspora* is an obligate or facultative endosymbiont is not known. Physical or chemical signals can induce *Capsaspora* cells to aggregate into round, 3-dimensional multicellular structures that require calcium for cell-cell adhesion (Ros-Rocher et al., 2023; Sebe-Pedros et al., 2013). Other filasterians and closely related organisms isolated from natural environments also form aggregates (Hehenberger et al., 2017; Tikhonenkov et al., 2020), indicating that aggregation is a conserved physiological process in this clade. *Capsaspora* is easily culturable in axenic medium, has a sequenced genome with chromosome-level assembly (Schultz et al., 2023; Suga et al., 2013), and is genetically tractable owing to gene disruption and stable transgenic techniques that we have recently developed (Phillips et al., 2022). Further, the *Capsaspora* genome contains many genes once thought specific to animals, such as cell-cell adhesion and ECM proteins (cadherins, integrins, and laminins) and developmental regulators (NF-κB, P53/63/73, Brachyury, and RUNX) (Suga et al., 2013). Therefore, along with other emerging holozoan research organisms (Booth and King, 2020; Faktorová et al., 2020; Kozyczkowska et al., 2021; Olivetta and Dudin, 2023; Woznica et al., 2021), *Capsaspora* is a valuable system for studying the function of such genes in unicellular organisms.

Previously, we have studied the role of the Hippo pathway in *Capsaspora* by generating a mutant of the single Yorkie/YAP/TAZ ortholog found in the genome (coYki) (Phillips et al., 2022). We found that coYki affects cytoskeletal dynamics, with coYki mutants showing constant ectopic blebbing at the cell cortex. Further, coYki affects the morphology of multicellular aggregates: whereas WT aggregates are spheroid, coYki mutant aggregates are flat and less circular than WT. Despite the well-characterized role of Yorkie/YAP/TAZ in promoting proliferation in animals, we saw no effect on cell proliferation in the coYki mutant, suggesting that regulation of proliferation by Yorkie/YAP/TAZ emerged after the last common ancestor of *Capsaspora* and animals. However, two important questions remain unanswered: 1) do the upstream components of the Hippo pathway regulate coYki, as they do in animals? 2) What effect does an increase of coYki activity have on *Capsaspora*?

In this study, we addressed these questions by generating homozygous mutant cell lines for the Hippo (coHpo) and Warts (coWts) kinases in *Capsaspora*. Loss of either kinase results in increased nuclear localization of coYki, showing that the regulatory activity of the Hippo kinase

cascade is conserved. Loss of coHpo or coWts does not increase cell proliferation, consistent with our previous conclusion that the Hippo pathway does not significantly affect proliferation in *Capsaspora*. However, loss of either kinase results in a distinct cytoskeletal phenotype: cells display a contractile behavior in which an initially round cell will elongate on an axis, adhere to the substrate at two terminal adhesion sites connected by an F-actin fiber, and then undergo contraction, returning to a round morphology. Further, we find that loss of these kinases increases the density of cell packing within multicellular aggregates, and we present evidence that this cell packing phenotype involves actomyosin-mediated contractile forces. Transgenic expression of a coYki mutant predicted to be hyperactive results in phenotypes like those observed in the coHpo and coWts mutants, suggesting that these phenotypes are caused by increased coYki activity due to a lack of kinase activity. Together, these results support our previous conclusions that the Hippo pathway regulates cytoskeletal dynamics but not proliferation in *Capsaspora*. In light of its well-established role in cell density-regulated proliferation control in animals, we speculate that the Hippo pathway may represent an ancient mechanism of cell density control preceding the emergence of animal multicellularity.

## RESULTS

### The Hippo pathway kinases regulate the subcellular localization of coYki in *Capsaspora*

Characterizing the function of the Hippo pathway in close unicellular relatives of animals may a) enhance our understanding of the evolutionary origins and ancestral function of this pathway and b) provide a relatively simple system to better understand how this biomedically significant pathway is regulated. To address these aims, we generated homozygous mutant cell lines for the single *Capsaspora* orthologs of the Hippo/MST and Warts/LATS kinases (coHpo and coWts, respectively.) For each gene, homologous recombination was used to replace the kinase domain of both WT alleles with selectable markers (Figure S1) as described previously (Phillips et al., 2022). Homozygous mutation of the kinases was verified by PCR and by sequencing the disrupted region of the genes (Figure 1- figure supplement 1).

In animals, the Hippo kinase cascade regulates the transcriptional coactivator Yorkie/YAP/TAZ by phosphorylation-mediated cytoplasmic sequestration (Dong et al., 2007). To test if the Hippo kinase cascade similarly regulates the subcellular localization of the single YAP/TAZ/Yorkie orthologue in *Capsaspora* (coYki), we transiently co-transfected WT, *coHpo-/-*, and *coWts-/-* cells with the fluorescent fusion proteins mScarlet-coYki and Histone H2B-Venus, a marker of the nucleus. In WT cells, mScarlet-coYki was predominantly cytoplasmic (Figure 1C), as reported previously (Phillips et al., 2022). In contrast, the majority of *coHpo-/-* and *coWts-/-* cells showed nuclear levels of mScarlet-coYki greater than or equal to that seen in the cytoplasm (Figure 1C and D). Interestingly, we found that *coWts-/-* cells were significantly more likely to show nuclear mScarlet-coYki localization than *coHpo-/-* cells (Figure 1D), which is consistent with Hpo/MST-independent activity of Wts/LATS previously reported in *Drosophila* and mammals (Zheng et al., 2015). Together, these results show that the *Capsaspora* Hippo kinase cascade regulates coYki by cytoplasmic sequestration, indicating a premetazoan origin of this regulatory activity of the Hippo pathway.

### The Hippo pathway kinases do not restrict cell proliferation in *Capsaspora*

The Hippo pathway negatively regulates tissue size and cell proliferation by restricting the activity of the growth-promoting oncogene Yorkie/YAP/TAZ in animals. However, we have previously reported that *coYki* is genetically dispensable for cell proliferation in *Capsaspora* (Phillips et al.,

2022). To further evaluate the role of proliferation control by the Hippo pathway in *Capsaspora*, we examined the requirement of *coHpo* and *coWts* in cell proliferation control under three distinct conditions: adherent growth while attached to a solid substrate, proliferation in shaking culture, and proliferation within multicellular aggregates. In adherent growth conditions, *coWts*-/- and *coHpo*-/- cells proliferated at similar rates as WT cells (Figure 2A). In shaking culture, *coHpo-/-* cells proliferated at similar rates as WT cells, whereas *coWts-/-* cells proliferated slower than WT (Figure 2B). As cells lacking a negative regulator of proliferation are expected to proliferate faster than WT cells, this result suggests that coWts is not a negative regulator of cell proliferation as in *Drosophila* and mammals, but instead is required for normal cell viability under some growth conditions. Finally, to examine cell proliferation within multicellular aggregates, we used EdU labeling, a marker of cells that have undergone S phase. The percentage of cells labeled by EdU in *coHpo-/-* and *coWts-/-* aggregates was not significantly different from WT aggregates (Figure 2C and D), indicating that coHpo and coWts do not affect cell proliferation within multicellular aggregates. Together with our previous characterization of *coYki* (Phillips et al., 2022), these results support the view that the Hippo pathway does not restrict cell proliferation in *Capsaspora* as in *Drosophila* and mammals.

**The Hippo pathway kinases regulate cell morphology and actomyosin-dependent contractile behaviors in *Capsaspora***

We have previously shown that, in contrast to WT *Capsaspora* cells with a round and relatively stable actin cortex, *coYki-/-* cells show aberrant, actin-depleted bleb-like protrusions at the cell cortex, implicating coYki in the control of cytoskeletal dynamics and cell morphology (Phillips et al., 2022). To test whether the Hippo pathway kinases affect the same processes in *Capsaspora,* we examined the morphology of adherent *coHpo-/-* and *coWts-/-* cells. While most cells showed a round cell body morphology (Figure 3A), a distinct elongated cell morphology was observed in a subset of *coWts* -/- or *coHpo* -/- cells, which was seen much less frequently in WT cells. Quantification of cellular aspect ratio in cell populations showed a non-gaussian distribution, with a distinct population of high aspect ratio cells in *coHpo* or *coWts* mutants (Figure 3B). The presence of elongated cells was rescued by transgenic expression of coHpo or coWts in the respective mutant (Figure 3A and B), demonstrating that the elongated cell phenotype was specifically due to the absence of these kinases.

189 To examine the dynamic properties of these elongated cells, we imaged *coHpo -/-* and *coWts -/-*
190 cells by time-lapse microscopy (Figure 3C and Videos S1-S3). These elongated cells are highly
191 dynamic. A previously round, motile cell starts extending along an axis, the direction of which
192 does not necessarily correspond with the cell's previous direction of movement. The cell then
193 stops extending, remaining for approximately 20 seconds in its elongated form. Filopodia appear
194 enriched at the poles of elongated cells (Figure 3C, 2:00 timepoint). To examine filopodia more
195 carefully, we stably expressed NMM-Venus in cells, which labels the cell membrane and allows
196 for visualization of the filopodia (Parra-Acero et al., 2018). Filopodia were enriched at the poles
197 of elongated cells in all genotypes (Figure 3 figure supplement 1), suggesting that filopodia may
198 play a role in this elongated morphology. After this elongated form, the cell then contracts:
199 adhesion at one of the poles is apparently lost, leading to a rapid contractile movement toward
200 the other pole and returning the cell to the initial round morphology. Together, these results
201 suggest that *Capsaspora* cells can perform a dynamic contractile behavior that is regulated by
202 the Hippo pathway kinases.
203
204 The actomyosin cytoskeletal network mediates amoeboid motion and cytokinesis in unicellular
205 organisms and contractile processes such as muscle contraction in animals (Brunet and Arendt,
206 2016). To examine the behavior of the actomyosin network in contractile *Capsaspora* cells, we
207 stably expressed Lifeact-mScarlet, which labels F-actin in *Capsaspora* cells (Phillips et al., 2022).
208 As contractile cells in the *coHpo* mutant background tended to show a more elongated
209 morphology than the *coWts* mutant, we focused on the *coHpo* mutant for further analysis. We
210 have previously reported that adherent WT *Capsaspora* cells show F-actin-rich foci near the area
211 of contact with the substrate. In motile cells, these foci do not move relative to the substrate,
212 suggesting that they are points of adhesion (Phillips et al., 2022). Similar F-actin-rich foci were
213 observed at or near the polar ends of elongated *coHpo -/-* cells (Figure 4A, blue arrowheads). In
214 most elongated cells, an F-actin fiber running parallel to the axis of elongation was observed
215 connecting the two polar foci (Figure 4A, yellow arrow; Videos S4-S5). During the contractile
216 process, the cell contracts towards one of the foci, which remains intact, while the other substrate-
217 foci interaction is lost, and the cell resumes a round morphology.
218
219 Superficially, the actin fibers observed in elongated *coHpo -/-* cells resemble stress fibers, which
220 are contractile cytoskeletal structures found in animal cells with functions in processes such as
221 extracellular matrix remodeling and cell motility (Tojkander et al., 2012). Contractility of stress
222 fibers is generated by the motor protein myosin II (Chrzanowska-Wodnicka and Burridge, 1996).

223 If myosin mediates the contractile behavior of *coHpo -/-* cells, then inhibition of myosin activity
224 may slow or prevent the contraction of elongated cells, resulting in more cells with an elongated
225 morphology in a population. To test this prediction, we treated cells with the myosin inhibitor
226 blebbistatin and then examined the occurrence of elongated cell morphology. Blebbistatin
227 treatment increased the occurrence of elongated cell morphology in *coHpo -/-* cell populations
228 (Figure 4B and C). Interestingly, despite the rarity of elongated cell morphology in WT cell
229 populations, blebbistatin also resulted in greatly increased occurrence of this morphology in WT
230 cell populations (Figure 4B and C). These results suggest that the contractile behavior of
231 *Capsaspora* cells is mediated by myosin activity.
232
233 **The Hippo pathway kinases regulate the density of cell packing in *Capsaspora* aggregates**
234 **via actomyosin-mediated contractility**
235
236 *Capsaspora* cells can aggregate into three-dimensional multicellular structures. We have
237 previously identified a critical role for coYki in this process: whereas WT *Capsaspora* cells form
238 round, spheroid aggregates, *coYki-/-* cells form asymmetrical and flattened aggregates (Phillips
239 et al., 2022). To test whether the Hippo pathway kinases regulate aggregate morphology, we
240 induced aggregate formation and then measured the size and circularity of aggregates. *coHpo -*
241 */-* aggregates showed similar size and circularity as WT aggregates (Figure 5A and B). However,
242 *coWts -/-* aggregates, while similar in size to WT, showed reduced circularity. Whereas WT
243 aggregates showed a round, smooth boundary, *coWts -/-* aggregate boundaries were rough and
244 showed nonuniform protrusions (Figure 5A and B). These results suggest that Hippo signaling
245 through coWts can affect aggregate morphology, but inactivation of the upstream Hippo kinase
246 alone is not sufficient to induce this effect.
247
248 *Capsaspora* aggregates are composed of adherent cells that form connections primarily through
249 filopodia-like protrusions on the cell surface. This can be visualized by mosaic aggregates
250 consisting of cells expressing mScarlet, which labels the cell body, and cells expressing NMM-
251 Venus, which allows for visualization of filopodia. In mosaic aggregates, contacts are visible
252 between filopodia but not between cell bodies (Figure 5C), showing that filopodium-filopodium
253 contacts, but not cell body to cell body contacts, are the primary mode of adhesion in aggregates.
254
255 While examining aggregate morphology, we noticed that *coHpo -/-* aggregates appeared more
256 opaque than WT, suggesting that the Hippo pathway kinases may affect the internal structure of

257 aggregates. To investigate this further, we stably expressed mScarlet in WT, *coHpo -/-*, *coWts -/-*
258 , and *coYki -/-* cells and then used optical sectioning to examine aggregate inner structure. This
259 analysis revealed that cells within *coHpo -/-* or *coWts -/-* aggregates appeared more tightly packed
260 than WT (Figure 5D). To quantify this effect, we measured the number of cells per unit area in
261 optical sections of aggregates. Whereas the number of cells per unit area in *coYki -/-* aggregates
262 was not significantly different from WT, the number of cells per area in *coHpo -/-* and *coWts -/-*
263 was significantly increased relative to WT (Figure 5E). These results indicate that loss of the Hippo
264 pathway kinases increases cell density within *Capsaspora* aggregates.
265
266 Filopodia mediate the adhesion between cells within aggregates (Figure 5C). To test whether
267 differences in filopodial morphology may underlie differences in aggregate shape or cell density
268 in the *coHpo* or *coWts* mutants, we generated mosaic aggregates consisting of WT and mutant
269 cells stably expressing distinct fluorescent labels that allow visualization of filopodia. This
270 mosaicism allowed us to examine the filopodia of individual cells within aggregates. Whereas
271 filopodia from *coHpo -/-* cells resembled those of WT and often extended more than a cell
272 diameter distance within the aggregate, filopodia from *coWts -/-* cells were much shorter (Figure
273 5 figure supplement 1). These results suggest that *coWts* affects the morphology of filopodia
274 within aggregates and that differences in filopodia-mediated interactions between cells may
275 underlie the aberrant shape of *coWts -/-* mutant aggregates (Figure 5A). However, as both *coHpo*
276 *-/-* and coWts -/- aggregates show increased cell density within aggregates, but *coHpo -/-* filopodia
277 do not appear different from WT filopodia, these results suggest that increased cell density is not
278 due to differences in filopodial morphology, but instead may be due to mechanical properties of
279 cells.
280
281 Given that *coHpo* and *coWts* regulate a contractile behavior in *Capsaspora* cells, a plausible
282 explanation for the increased cell packing within *coHpo -/-* and *coWts -/-* aggregates is that an
283 increase in intercellular contractile interactions pulls cells closer and therefore leads to increased
284 cell density in mutant aggregates. To test whether actomyosin-mediated contractile forces affect
285 cell packing within aggregates, we treated WT and *coHpo -/-* aggregates with the myosin II
286 inhibitor blebbistatin or the actin-depolymerizing drug latrunculin B (LatB). For both WT and *coHpo*
287 *-/-* aggregates, treatment with either blebbistatin or LatB decreased cell density within aggregates,
288 as reflected by a reduction in the number of cells per unit area (Figure 6A-D). Together, these
289 results suggest that the Hippo pathway kinases regulate the density of cell packing in *Capsaspora*
290 aggregates via actomyosin-mediated contractility .

291

292 *coYki* affects both the cytoskeletal dynamics of *Capsaspora* cells and the shape of multicellular
293 aggregates (Phillips et al., 2022). Given these previous results and the fact that Yorkie/YAP/TAZ
294 is inhibited by the Hippo pathway kinases in other organisms, it is plausible that the phenotypes
295 observed in the *coHpo* and *coWts* mutants are mediated by *coYki.* Since techniques are currently
296 unavailable to create double mutants in *Capsaspora*, we could not test this possibility through
297 classic genetic epistasis. As an alternative approach, we asked whether ectopic activation of
298 *coYki* can phenocopy the loss of *coHpo* or *coWts*, by transgenically expressing a coYki mutant in
299 which the four predicted Wts/LATS phosphorylation sites are mutated to non-phosphorylatable
300 Alanine (coYki 4SA). coYki 4SA shows increased nuclear localization compared to the wild-type
301 coYki protein (Phillips et al., 2022), and thus is predicted to be hyperactive. As observed in *coHpo*
302 and *coWts* mutants, stable transgenic expression of coYki 4SA resulted in increased cell packing
303 of *Capsaspora* aggregates (Figure 7 A and B), as well as an elongated cell morphology in
304 adherent cells (Figure 7 C and D). These results suggest that the phenotypes observed in *coHpo*
305 and *coWts* mutants are due to coYki activation resulting from a loss of upstream kinase signaling.
306

307 Previously, Xu et al. reported that in *Drosophila*, Yorkie can act in a transcription-independent
308 manner at the cell cortex to regulate actomyosin-mediated contractility (Xu et al., 2018), raising
309 the possibility that cytoskeletal regulation by coYki is transcription independent. To test this
310 possibility, we evaluated whether coYki 4SA requires transcriptional activity to affect cell and
311 aggregate morphology. The conserved coYki residue F123 aligns with the human YAP1 residue
312 F95, which is required for YAP-TEAD binding and YAP transcriptional activity (Li et al., 2010).
313 The analogous residue in *Drosophila* is not required for the transcription-independent Yorkie
314 activity reported by Xu et al. (Xu et al., 2018). We found that, in contrast to coYki 4SA, expression
315 of a coYki 4SA F123A mutant did not affect cell or aggregate morphology (Figure 7). This result
316 indicates that these phenotypes are mediated by the transcriptional activity of coYki.
317

318 **Effects of the Hippo pathway on gene expression in *Capsaspora***
319

320 To better understand how perturbation of Hippo pathway signaling affects gene expression in
321 *Capsaspora*, we performed RNA-seq on *coHpo -/-* and *coWts -/-* cells. We previously identified
322 15 *Capsaspora* genes differentially expressed in the *coYki -/-* mutant that are predicted to bind
323 actin (Phillips et al., 2022). Of these genes, 14 were differentially expressed in the *coHpo* or coWts
324 mutant cell lines, and 6 of these genes were differentially expressed in both the *coHpo* and *coWts*

325 mutant lines (Differences in gene expression between WT and mutant are significant, with $p <$
326 $0.05$ (Supplementary File 1)). This result indicates that *coYki*, *coHpo*, and *coWts* regulate a
327 shared set of genes, a subset of which may affect cytoskeletal properties of cells through actin
328 regulation.
329
330 To further examine how the Hippo pathway affects gene expression in *Capsaspora*, we performed
331 functional enrichment analysis on three gene sets: genes differentially expressed in the *coHpo*
332 mutant (1032 genes), the *coWts* mutant (609 genes), and the overlapping set of genes
333 differentially expressed in the *coHpo*, *coWts*, and *coYki* mutants (107 genes, termed the "core
334 Hippo pathway" gene set) using *coYki* mutant sequencing data from our previous study (Phillips
335 et al., 2022)(See Supplementary File 2 for gene lists). The core Hippo pathway set showed
336 enrichment in membrane-associated and transmembrane domain-containing proteins, proteins
337 functionally linked to differentiation, and proteins encoding a laminin G domain (Figure 8).
338 Laminins are a component of the ECM in animals, functioning to couple cell surface receptors
339 such as integrins to the basement membrane (Hohenester and Yurchenco, 2013). The function
340 of Laminin G domain-containing *Capsaspora* proteins is unknown, and conservation of this
341 domain appears restricted to animals and their closest unicellular relatives such as filasterians
342 and choanoflagellates (Fahey and Degnan, 2012; Williams et al., 2014). Another protein domain,
343 Insulin-like growth factor binding protein, N-terminal (IGFBPN), was also enriched in the core
344 Hippo pathway gene set. In animals, this domain is associated with receptor tyrosine kinases and
345 other proteins linked to tyrosine kinase signaling (Ward et al., 1995; Zeslawski et al., 2001). The
346 sets of genes differentially expressed in the coHpo or coWts mutants also showed enrichment in
347 genes encoding the IGFBPN domain, membrane-associated proteins, and genes functionally
348 linked to differentiation (Figure 8- figure supplement 1). The finding that the *Capsaspora* Hippo
349 pathway regulates genes encoding membrane proteins and putative ECM components such as
350 laminins suggests that this pathway may regulate cell and aggregate morphology not just through
351 intracellular cytoskeletal regulators, but also through modification of the extracellular environment
352 and cell surface proteins such as receptors or adhesion molecules.
353

354 **Discussion**

355

356 The evolutionary process by which the signaling pathways that regulate animal development
357 came to function in these roles remains unclear. Apart from shedding light on the origin of animals,
358 knowledge about this process could provide a deeper understanding of these signaling pathways,
359 which play key roles in human health and disease. Although we cannot study the ancestral
360 unicellular organisms that gave rise to animals, studying modern close unicellular relatives of
361 animals can guide our understanding of what these organisms may have been like, and how
362 conserved signaling pathways may have functioned in these unicellular ancestors. Our previous
363 characterization of the Yorkie/YAP/TAZ ortholog coYki in *Capsaspora* showed that coYki affects
364 actin dynamics and the shape of multicellular aggregates in this close unicellular relative of
365 animals. However, we saw no effect on proliferation in the coYki mutant, suggesting that
366 regulation of proliferation by Yorkie/YAP/TAZ may have evolved later in the lineage leading to
367 animals. In this report, we build on our previous study by assessing the function of the upstream
368 kinases coHpo and coWts in *Capsaspora*. We find that the mechanism of Yorkie/YAP/TAZ
369 regulation (specifically, cytoplasmic sequestration by an upstream kinase cascade consisting of
370 Hippo and Warts kinases) is conserved in *Capsaspora* and animals, indicating an ancient origin
371 of this signaling machinery. These findings support and extend our previous study uncovering a
372 role for Hippo signaling in the regulation of cytoskeletal dynamics but not cell proliferation.
373 Together, our studies suggest that the ancestral function of the Hippo pathway was cytoskeletal
374 regulation, and that subsequently the pathway was co-opted to regulate cell proliferation and
375 tissue size in animals.

376

377 In this report, we describe a contractile cell behavior observed in *coHpo* and *coWts* mutants. In
378 this process, the cell transitions from a round morphology to an elongated spindle shape. The cell
379 will remain in the spindle shape for approximately 20 seconds and then contract towards one
380 pole. We interpret this as a process in which cells extend and then adhere to the substrate at the
381 two ends of the spindle, contractile forces within the cell increase, and adhesion at one of the
382 poles is subsequently lost, leading to contraction towards the other pole. Visualization of actin in
383 live cells is consistent with this model: we observed actin-rich foci at the adhesive sites at the
384 poles of spindle-shaped cells, and an actin filament connecting these foci, which may serve as a
385 tension-generating structure. The cytoskeletal structures that we observe resemble
386 adhesive/contractile structures in mammalian cells such as podosomes (Linder et al., 2023), focal
387 adhesions (Fierro Morales et al., 2022), and stress fibers (Tojkander et al., 2012). As *Capsaspora*

388 encodes orthologs of some proteins known to label these structures, future colocalization
389 experiments may reveal the degree of conservation between such subcellular structures in
390 *Capsaspora* and animals.
391
392 The function of these contractile cells is presently unclear. While we observed the contractile
393 behavior on glass surface, which is non-physiological, we speculate that such contraction exerted
394 on a pliable surface may remodel a cell's extracellular environment to provide certain fitness
395 benefits. Intriguingly, the elongated, spindle morphology was reported to be common (nearly 50
396 percent of cells) after isolation of *Capsaspora* cells from the *B. glabrata* snail host (Stibbs et al.,
397 1979), suggesting that environmental factors from the snail host may affect this elongated
398 morphology and potentially Hippo pathway signaling. We further speculate that increased
399 contractility within multicellular aggregates may serve to pull the neighboring cells closer to each
400 other, which may contribute to the increased packing in the of *coHpo* or *coWts* mutant aggregates.
401 Given that the elongated cell morphology is rarely but occasionally observed in the WT
402 background, an interesting possibility is that coYki is transiently activated in these cells. Further
403 studies utilizing in vivo reporters of coYki activity may reveal whether this is the case.
404
405 We show that the elongated cell morphology visible in *coHpo* and *coWts* mutants becomes more
406 common after treatment with blebbistatin, indicating a role for myosin II in the contraction of this
407 elongated cell state. One interpretation of the increase in elongated cells in the *coHpo* and *coWts*
408 mutants, therefore, is that myosin activity is reduced. However, we also see that blebbistatin
409 treatment reduces the packing of cells within multicellular groups, whereas loss of *coHpo* or *coWts*
410 causes an increase in cell packing. Thus the specific role of myosin activity in the phenotypes
411 observed in Hippo pathway mutants in *Capsaspora* remains unclear. One possibility is that the
412 initial process of cell elongation is unrelated to myosin, and it is this process that is enhanced in
413 *coHpo* and *coWts* mutants. Although techniques to visualize and quantify myosin activity in
414 *Capsaspora* have not been developed, future work in this regard could elucidate the relationship
415 between myosin activity and Hippo signaling in *Capsaspora.*
416
417 Previous work has examined the structure of *Capsaspora* aggregates by electron microscopy
418 (Sebe-Pedros et al., 2013). In this report we have furthered our understanding of aggregate
419 structure by providing evidence that a) cells within aggregates appear to contact their neighbors
420 largely by interactions between filopodia; and b) Hippo pathway activity affects the packing of
421 cells within these aggregates. In animals, the predominant form of multicellular structure is

422 epithelia, in which cells with apical-basal polarity form lateral contacts at adherens junctions,
423 septate junctions, tight junctions, and desmosomes (Abedin and King, 2010). However,
424 microvilli/filopodial adhesion plays important roles in dorsal closure in *Drosophila* (Jacinto et al.,
425 2000), early embryo compaction in mouse (Fierro-Gonzalez et al., 2013), and other
426 developmental processes (Brunet and Booth, 2023). Further, inter-microvillar contacts are the
427 apparent means of adherence in the choanoflagellate *C. flexa,* another close unicellular relative
428 of animals, that can exist in a sheet-like morphology with a remarkable actomyosin-dependent
429 inverting activity (Brunet et al., 2019). Thus microvilli/filopodia-mediated adhesion may be an
430 ancient and conserved means of multicellularity that preceded the formation of epithelia.
431
432 In cultured mammalian cells, Hippo signaling regulates contact inhibition, a phenomenon in which
433 proliferation is arrested upon cell confluency to achieve a proper cell density (Aragona et al., 2013;
434 Zhao et al., 2007). Interestingly, while Hippo signaling does not regulate cell proliferation in
435 *Capsaspora*, loss of Hippo pathway kinases or increase in coYki activity increases the density of
436 cell packing within *Capsaspora* aggregates. Thus, despite the distinct routes of achieving proper
437 cell density (cell proliferation vs. cell aggregation), the Hippo pathway appears to restrict cell
438 density in both animals and *Capsaspora*. We speculate that the Hippo pathway may represent an
439 ancient mechanism of cell density control preceding the emergence of animal multicellularity.
440 Significantly, this model suggests that the signals that regulate the Hippo pathway in animals and
441 *Capsaspora* may be conserved, and therefore studying *Capsaspora* could provide important
442 insights into the regulation of this biomedically significant pathway.
443

444 **MATERIALS AND METHODS**

445

| Key Resources Table | | | | |
|---|---|---|---|---|
| **Reagent type (species) or resource** | **Designation** | **Source or reference** | **Identifiers** | **Additional information** |
| gene (*Capsaspora owczarzaki*) | *coHpo* | Genbank | CAOG_01932 | |
| gene (*Capsaspora owczarzaki*) | *coWts* | Genbank | CAOG_00619 | |
| gene (*Capsaspora owczarzaki*) | *coYki* | Genbank | CAOG_07866 | |
| cell line (*Capsaspora owczarzaki*) | WT | ATCC | 30864 | |
| recombinant DNA reagent | pJP80 | (Phillips et al., 2022) | | *Capsaspora* expression vector: mScarlet-coYki fusion, Geneticin resistance |
| recombinant DNA reagent | pONSY-coH2B:Venus | Addgene | Addgene Plasmid #111877 | *Capsaspora* expression vector: Histone H2B-Venus fusion |
| recombinant DNA reagent | pJP122 | This paper | | *Capsaspora* expression vector: coHpo transgene, Hygromycin B Resistance |
| recombinant DNA reagent | pJP125 | This paper | | *Capsaspora* expression vector: coWts transgene, Hygromycin B Resistance |
| recombinant DNA reagent | pJP145 | This paper | | *Capsaspora* expression vector: NMM-Venus, Hygromycin B Resistance |

| | | | | |
|---|---|---|---|---|
| recombinant DNA reagent | pJP118 | (Phillips et al., 2022) | | *Capsaspora* expression vector: Lifeact-mScarlet, Hygromycin B Resistance |
| recombinant DNA reagent | pJP103 | (Phillips et al., 2022) | | *Capsaspora* expression vector: mScarlet, Hygromycin B Resistance |
| recombinant DNA reagent | pJP90 | (Phillips et al., 2022) | | *Capsaspora* expression vector: coYki 4SA , Geneticin Resistance |
| sequence-based reagent | oJP201: coHpo KO Forward: homologous arm + actin promoter | This paper | PCR primers | CCCGCCTCGTCCCAACAAC AGCTCGTACGGCTCGGTCT TCAAGGCTCGCCACAAGGA CACCCAGTCCATCCTCGCC GTCAAGCAGGTGCCCCTTG AGAAC**ACAAAAATGCTGAT TGTTTG** |
| sequence-based reagent | oJP202: coHpo KO Reverse: homologous arm + actin terminator | This paper | PCR primers | AAGCAACATTGCTTCGTTG ACTAACGCTTCATGGTGCC GTCCTCGCCCATGACCATC GTGCCGGAGTCGCCAGTG ACCATCGTTCCGCTATCAA CAAGGG**TTTTTTCTTTGTAC AAGATCAC** |
| sequence-based reagent | oJP203: coWts KO Forward: homologous arm + actin promoter | This paper | PCR primers | CAAACGGCGAGACCAGCT CGAGATTGAGATGGCCAAG ATGGACCTGACCGATGTTC AAAAGACCCAGTTGCGTCG CATCCTCCGCATGAAGGAA TCAGAG**ACAAAAATGCTGA TTGTTTG** |
| sequence-based reagent | oJP204: coWts KO Reverse: homologous arm + actin terminator | This paper | PCR primers | GCATTTTAATGTGCTCGAC CGTCTCCCGGCCGAGACG ATCGGAGGATTCACAGCAG AGCCGGGAGATGAGGTCTT TGGACTCGCGCGAAATCTT TGCCCG**TTTTTTCTTTGTAC AAGATCAC** |
| sequence-based reagent | oJP205: coHpo Diagnostic Forward | This paper | PCR primers | CAAAAACAACAGCGAAAAC G |

| | | | | |
|---|---|---|---|---|
| sequence-based reagent | oJP206: coHpo Diagnostic Reverse | This paper | PCR primers | CCATCGGAGGAAACTAAAGG |
| sequence-based reagent | oJP207: coWts Diagnostic Forward | This paper | PCR primers | TGCTGCTGAAAATGAAAACG |
| sequence-based reagent | oJP208: coWts Diagnostic Reverse | This paper | PCR primers | GAACCTCACCAGGATTTTGC |
| commercial assay or kit | TransIT-X2 Dynamic Delivery System | Mirus Bio | MIR 6003 | |
| commercial assay or kit | Click-iT™ Plus EdU Cell Proliferation Kit for Imaging, Alexa Fluor™ 488 dye | ThermoFisher | C10637 | |
| chemical compound, drug | Blebbistatin | Sigma-Aldrich | B0560 | |
| chemical compound, drug | Latrunculin B | Sigma-Aldrich | L5288 | |

446
447
448

449 Cell culture

450 *Capsaspora* cells were grown in ATCC medium 1034 as described previously (Phillips et al.,
451 2022). Quantification of proliferation in shaking culture, induction of aggregates, quantification of
452 aggregate size and circularity, EdU labeling within aggregates, and quantification of mScarlet-
453 coYki fluorescence intensity were done as described previously (Phillips et al., 2022).
454 Quantification of proliferation on a solid substrate was done as described previously (Phillips et
455 al., 2022), except 96-well plates were used in place of 24-well plates. To add blebbistatin (Sigma
456 B0560) or latrunculin B (Sigma L5288) to cell cultures, a 10X mix of drug or vehicle control in
457 growth medium was prepared, and this concentrated drug preparation was added to cultures so
458 that a final 1X concentration of drugs was reached.

459

460 Molecular Biology

461 For a list of plasmids and oligonucleotides generated for this study, see Key Resources Table.
462 For a list of synthesized DNA sequences used in this study, see Supplementary File 3. For
463 transgenic expression of *Capsaspora* genes, we synthesized genes coding for the appropriate
464 *Capsaspora* protein but with synonymous codon changes throughout the DNA sequence. This
465 was done to reduce DNA sequence homology in order to prevent homologous recombination of
466 the transgene with the endogenous *Capsaspora* alleles during plasmid integration into the
467 genome, as done previously (Phillips et al., 2022). To construct a plasmid for transgenic
468 expression of coHpo in *Capsaspora* cells (pJP122), we synthesized a transgene encoding the
469 coHpo protein (sJP201). There are three predicted isoforms of the coHpo sequence, but only one
470 of these encodes the SARAH domain, which is important for Hippo kinase activity in Hippo
471 pathway signaling (Scheel and Hofmann, 2003). We therefore used the isoform sequence
472 encoding the SARAH domain to design our transgene. The coHpo transgene was cloned into a
473 KpnI and AflII digest of pJP103 (Addgene #176481) using Gibson assembly, generating a vector
474 encoding the coHpo transgene and hygromycin B resistance. Similarly, a coWts transgene was
475 synthesized (sJP202) and cloned into a KpnI and AflII digest of pJP103 by Gibson assembly,
476 generating a vector encoding a coWts transgene and hygromycin B resistance (pJP125.)

477

478 To generate a plasmid to stably express N-myristoylation motif (NMM)-Venus (pJP145), a marker
479 of the plasma membrane and filopodia in *Capsaspora*, we first constructed a vector expressing
480 both Venus and hygromycin B resistance (pJP115) by PCR-amplifying the Venus gene from
481 pJP114 (Phillips et al., 2022) and cloning it by Gibson assembly into a KpnI and AflII digest of
482 pJP103 (Addgene #176481), which contains a hygromycin B resistance cassette. We then

483 synthesized the NMM motif (sJP203) following the sequence from the pONSY-coNMM:mCherry
484 vector (Addgene #111878, (Parra-Acero et al., 2018)) and cloned this DNA fragment into a KpnI
485 digest of pJP115 using Gibson assembly.
486
487 *Capsaspora* transfection and genome editing
488 Transfection of *Capsaspora* cells and stable cell line generation was done using the *Trans*IT-X2
489 transfection reagent (Mirus Bio) as previously described (Phillips et al., 2022). Disruptions of
490 *Capsaspora* genes were done as previously described (Phillips et al., 2022). Briefly, oligos
491 oJP201 and oJP202 were used to generate gene targeting constructs by PCR with homologous
492 arms that target the coHpo gene (CAOG_01932). Oligos oJP203 and oJP204 were used to
493 generate gene-targeting constructs for the coWts gene (CAOG_00619). For both homozygous
494 mutants, the two WT alleles present in the diploid *Capsaspora* genome were disrupted using
495 selectable markers for geneticin resistance and nourseothricin resistance. oJP205 and oJP206
496 were used in a diagnostic PCR that amplifies across the deleted region of the *coHpo* gene, and
497 oligos oJP207 and oJP208 were used in a diagnostic PCR across the deleted region of the *coWts*
498 gene.
499
500 Measurement of cell and aggregate properties
501 To measure the aspect ratio of cells, the ImageJ freehand selection tool was used to manually
502 trace the border of imaged cells, and the Measure function was used to calculate the cellular
503 aspect ratio. To quantify cell packing within aggregates expressing mScarlet, a z-stack of optical
504 sections was obtained by confocal microscopy. To measure cells within the aggregate as opposed
505 to cells at the edge of the aggregate, an optical section 14 microns deep into the aggregate was
506 used for measurement. A 40 micron$^2$ square was drawn in the center of the optical section of the
507 aggregate and the number of cells in the square was counted.
508
509 RNA-seq
510 RNA-seq of *Capsaspora* cells was done as previously described (Phillips et al., 2022) except that
511 cells were inoculated into flasks at 4 x $10^5$ cells/ml instead of 2 x $10^5$ cells/ml to increase RNA
512 yield. Analysis of RNA-seq data was done as previously described (Phillips et al., 2022), except
513 that after differential expression analysis by edgeR (Robinson et al., 2010), the following criteria
514 were used to select genes for further analysis: false discovery rate [FDR] ≤ 0.001, absolute
515 log2(fold change) ≥ 0.5, log(counts per million) ≥ 0. Enrichment analyses were done using DAVID
516 (Sherman et al., 2022).

517

518 Gene nomenclature

519 In this article, we use italicized text to refer to a gene (e.g., *coHpo*), unitalicized text to refer to a
520 protein (e.g., coHpo), and '-/-' to indicate a homozygous deletion mutant (e.g., *coHpo -/-).* "*EF1 >*
521 *coHpo*" indicates transgenic expression of *coHpo* driven by the *EF1* promoter.

522

523 Statistics

524 Statistical analyses were done using Prism (GraphPad Software, San Diego, CA). For
525 experiments where multiple cells or aggregates were measured for each independent experiment,
526 the mean of all measurements made for each biological replicate was calculated, and statistical
527 analyses were performed on these sample level means following (Lord et al., 2020).

528

529 Data Availability

530 RNA-seq data generated in this study have been deposited into the NCBI SRA (BioProject
531 accession number PRJNA1060651).

532

533 **Acknowledgements:**

534 We thank Maribel Santos for technical assistance with genotyping cell lines. We thank Dr. Iñaki
535 Ruiz-Trillo for the gift of pONSY-coH2B:Venus vector (Addgene plasmid number 111877). This
536 work was supported in part by National Institute of Health grant EY015708 to D.P. During this
537 work J.E.P was a Howard Hughes Medical Institute fellow of the Life Sciences Research
538 Foundation. D.P. is an investigator of the Howard Hughes Medical Institute.

539

## REFERENCES


Abedin, M., and King, N. (2010). Diverse evolutionary paths to cell adhesion. Trends Cell Biol *20*, 734-742.

Aragona, M., Panciera, T., Manfrin, A., Giulitti, S., Michielin, F., Elvassore, N., Dupont, S., and Piccolo, S. (2013). A Mechanical Checkpoint Controls Multicellular Growth through YAP/TAZ Regulation by Actin-Processing Factors. Cell *154*, 1047-1059.

Booth, D.S., and King, N. (2020). Genome editing enables reverse genetics of multicellular development in the choanoflagellate Salpingoeca rosetta. Elife *9*.

Brunet, T., and Arendt, D. (2016). From damage response to action potentials: early evolution of neural and contractile modules in stem eukaryotes. Philos Trans R Soc Lond B Biol Sci *371*, 20150043.

Brunet, T., and Booth, D.S. (2023). Cell polarity in the protist-to-animal transition. Curr Top Dev Biol *154*, 1-36.

Brunet, T., Larson, B.T., Linden, T.A., Vermeij, M.J.A., McDonald, K., and King, N. (2019). Light-regulated collective contractility in a multicellular choanoflagellate. Science *366*, 326-334.

Chrzanowska-Wodnicka, M., and Burridge, K. (1996). Rho-stimulated contractility drives the formation of stress fibers and focal adhesions. J Cell Biol *133*, 1403-1415.

Deng, H., Wang, W., Yu, J., Zheng, Y., Qing, Y., and Pan, D. (2015). Spectrin regulates Hippo signaling by modulating cortical actomyosin activity. Elife *4*, e06567.

Dong, J., Feldmann, G., Huang, J., Wu, S., Zhang, N., Comerford, S.A., Gayyed, M.F., Anders, R.A., Maitra, A., and Pan, D. (2007). Elucidation of a universal size-control mechanism in Drosophila and mammals. Cell *130*, 1120-1133.

Dupont, S., Morsut, L., Aragona, M., Enzo, E., Giulitti, S., Cordenonsi, M., Zanconato, F., Le Digabel, J., Forcato, M., Bicciato, S.*, et al.* (2011). Role of YAP/TAZ in mechanotransduction. Nature *474*, 179-183.

Fahey, B., and Degnan, B.M. (2012). Origin and evolution of laminin gene family diversity. Mol Biol Evol *29*, 1823-1836.

Faktorová, D., Nisbet, R.E.R., Robledo, J.A.F., Casacuberta, E., Sudek, L., Allen, A.E., Ares, M., Aresté, C., Balestreri, C., Barbrook, A.C.*, et al.* (2020). Genetic tool development in marine protists: emerging model organisms for experimental cell biology. Nature Methods *17*, 481-+.

571 Fierro Morales, J.C., Xue, Q., and Roh-Johnson, M. (2022). An evolutionary and physiological
572 perspective on cell-substrate adhesion machinery for cell migration. Front Cell Dev Biol *10*,
573 943606.

574 Fierro-Gonzalez, J.C., White, M.D., Silva, J.C., and Plachta, N. (2013). Cadherin-dependent
575 filopodia control preimplantation embryo compaction. Nat Cell Biol *15*, 1424-1433.

576 Hamaratoglu, F., Willecke, M., Kango-Singh, M., Nolo, R., Hyun, E., Tao, C., Jafar-Nejad, H., and
577 Halder, G. (2006). The tumour-suppressor genes NF2/Merlin and Expanded act through Hippo
578 signalling to regulate cell proliferation and apoptosis. Nat Cell Biol *8*, 27-36.

579 Hehenberger, E., Tikhonenkov, D.V., Kolisko, M., Del Campo, J., Esaulov, A.S., Mylnikov, A.P.,
580 and Keeling, P.J. (2017). Novel Predators Reshape Holozoan Phylogeny and Reveal the
581 Presence of a Two-Component Signaling System in the Ancestor of Animals. Curr Biol *27*, 2043-
582 2050 e2046.

583 Hohenester, E., and Yurchenco, P.D. (2013). Laminins in basement membrane assembly. Cell
584 Adh Migr *7*, 56-63.

585 Jacinto, A., Wood, W., Balayo, T., Turmaine, M., Martinez-Arias, A., and Martin, P. (2000).
586 Dynamic actin-based epithelial adhesion and cell matching during Drosophila dorsal closure.
587 Current Biology *10*, 1420-1426.

588 Kozyczkowska, A., Najle, S.R., Ocana-Pallares, E., Areste, C., Shabardina, V., Ara, P.S., Ruiz-
589 Trillo, I., and Casacuberta, E. (2021). Stable transfection in protist Corallochytriumlimacisporum
590 identifies novel cellular features among unicellular animals relatives. Curr Biol.

591 Li, Z., Zhao, B., Wang, P., Chen, F., Dong, Z., Yang, H., Guan, K.L., and Xu, Y. (2010). Structural
592 insights into the YAP and TEAD complex. Genes Dev *24*, 235-240.

593 Linder, S., Cervero, P., Eddy, R., and Condeelis, J. (2023). Mechanisms and roles of podosomes
594 and invadopodia. Nat Rev Mol Cell Biol *24*, 86-106.

595 Lord, S.J., Velle, K.B., Mullins, R.D., and Fritz-Laylin, L.K. (2020). SuperPlots: Communicating
596 reproducibility and variability in cell biology. J Cell Biol *219*.

597 Ma, S., Meng, Z., Chen, R., and Guan, K.L. (2019). The Hippo Pathway: Biology and
598 Pathophysiology. Annu Rev Biochem *88*, 577-604.

599 Olivetta, M., and Dudin, O. (2023). The nuclear-to-cytoplasmic ratio drives cellularization in the
600 close animal relative Sphaeroforma arctica. Curr Biol *33*, 1597-1605 e1593.

601 Pan, D. (2022). The unfolding of the Hippo signaling pathway. Dev Biol *487*, 1-9.

602 Parra-Acero, H., Ros-Rocher, N., Perez-Posada, A., Kozyczkowska, A., Sanchez-Pons, N.,
603 Nakata, A., Suga, H., Najle, S.R., and Ruiz-Trillo, I. (2018). Transfection of Capsaspora
604 owczarzaki, a close unicellular relative of animals. Development *145*.

605 Patterson, D.J., Nygaard, K., Steinberg, G., and Turley, C.M. (1993). Heterotrophic Flagellates
606 and Other Protists Associated with Oceanic Detritus Throughout the Water Column in the Mid
607 North-Atlantic. J Mar Biol Assoc Uk *73*, 67-95.

608 Phillips, J.E., Santos, M., Konchwala, M., Xing, C., and Pan, D. (2022). Genome editing in the
609 unicellular holozoan Capsaspora owczarzaki suggests a premetazoan role for the Hippo pathway
610 in multicellular morphogenesis. Elife *11*.

611 Robinson, M.D., McCarthy, D.J., and Smyth, G.K. (2010). edgeR: a Bioconductor package for
612 differential expression analysis of digital gene expression data. Bioinformatics *26*, 139-140.

613 Ros-Rocher, N., Kidner, R.Q., Gerdt, C., Davidson, W.S., Ruiz-Trillo, I., and Gerdt, J.P. (2023).
614 Chemical factors induce aggregative multicellularity in a close unicellular relative of animals. Proc
615 Natl Acad Sci U S A *120*, e2216668120.

616 Ros-Rocher, N., Perez-Posada, A., Leger, M.M., and Ruiz-Trillo, I. (2021). The origin of animals:
617 an ancestral reconstruction of the unicellular-to-multicellular transition. Open Biol *11*, 200359.

618 Scheel, H., and Hofmann, K. (2003). A novel interaction motif, SARAH, connects three classes of
619 tumor suppressor. Curr Biol *13*, R899-900.

620 Schultz, D.T., Haddock, S.H.D., Bredeson, J.V., Green, R.E., Simakov, O., and Rokhsar, D.S.
621 (2023). Ancient gene linkages support ctenophores as sister to other animals. Nature *618*, 110-
622 117.

623 Sebe-Pedros, A., Irimia, M., Del Campo, J., Parra-Acero, H., Russ, C., Nusbaum, C., Blencowe,
624 B.J., and Ruiz-Trillo, I. (2013). Regulated aggregative multicellularity in a close unicellular relative
625 of metazoa. Elife *2*, e01287.

626 Sebe-Pedros, A., Zheng, Y., Ruiz-Trillo, I., and Pan, D. (2012). Premetazoan origin of the hippo
627 signaling pathway. Cell Rep *1*, 13-20.

628 Shalchian-Tabrizi, K., Minge, M.A., Espelund, M., Orr, R., Ruden, T., Jakobsen, K.S., and
629 Cavalier-Smith, T. (2008). Multigene phylogeny of choanozoa and the origin of animals. PLoS
630 One *3*, e2098.

631 Sherman, B.T., Hao, M., Qiu, J., Jiao, X., Baseler, M.W., Lane, H.C., Imamichi, T., and Chang,
632 W. (2022). DAVID: a web server for functional enrichment analysis and functional annotation of
633 gene lists (2021 update). Nucleic Acids Res *50*, W216-W221.

634 Stibbs, H.H., Owczarzak, A., Bayne, C.J., and DeWan, P. (1979). Schistosome sporocyst-killing
635 Amoebae isolated from Biomphalaria glabrata. J Invertebr Pathol *33*, 159-170.

636 Suga, H., Chen, Z., de Mendoza, A., Sebe-Pedros, A., Brown, M.W., Kramer, E., Carr, M., Kerner,
637 P., Vervoort, M., Sanchez-Pons, N.*, et al.* (2013). The Capsaspora genome reveals a complex
638 unicellular prehistory of animals. Nat Commun *4*, 2325.

639 Tikhonenkov, D.V., Mikhailov, K.V., Hehenberger, E., Karpov, S.A., Prokina, K.I., Esaulov, A.S.,
640 Belyakova, O.I., Mazei, Y.A., Mylnikov, A.P., Aleoshin, V.V.*, et al.* (2020). New Lineage of
641 Microbial Predators Adds Complexity to Reconstructing the Evolutionary Origin of Animals. Curr
642 Biol *30*, 4500-4509 e4505.

643 Tojkander, S., Gateva, G., and Lappalainen, P. (2012). Actin stress fibers--assembly, dynamics
644 and biological roles. J Cell Sci *125*, 1855-1864.

645 Tong, S.M. (1997). Heterotrophic flagellates and other protists from Southampton Water, UK.
646 Ophelia *47*, 71-131.

647 Ward, C.W., Hoyne, P.A., and Flegg, R.H. (1995). Insulin and epidermal growth factor receptors
648 contain the cysteine repeat motif found in the tumor necrosis factor receptor. Proteins *22*, 141-
649 153.

650 Williams, F., Tew, H.A., Paul, C.E., and Adams, J.C. (2014). The predicted secretomes of
651 Monosiga brevicollis and Capsaspora owczarzaki, close unicellular relatives of metazoans, reveal
652 new insights into the evolution of the metazoan extracellular matrix. Matrix Biol *37*, 60-68.

653 Woznica, A., Kumar, A., Sturge, C.R., Xing, C., King, N., and Pfeiffer, J.K. (2021). STING
654 mediates immune responses in the closest living relatives of animals. Elife *10*.

655 Wu, S., Liu, Y., Zheng, Y., Dong, J., and Pan, D. (2008). The TEAD/TEF family protein Scalloped
656 mediates transcriptional output of the Hippo growth-regulatory pathway. Dev Cell *14*, 388-398.

657 Xu, J., Vanderzalm, P.J., Ludwig, M., Su, T., Tokamov, S.A., and Fehon, R.G. (2018). Yorkie
658 Functions at the Cell Cortex to Promote Myosin Activation in a Non-transcriptional Manner. Dev
659 Cell *46*, 271-284 e275.

660 Yang, C.C., Graves, H.K., Moya, I.M., Tao, C., Hamaratoglu, F., Gladden, A.B., and Halder, G.
661 (2015). Differential regulation of the Hippo pathway by adherens junctions and apical-basal cell
662 polarity modules. Proc Natl Acad Sci U S A *112*, 1785-1790.

663 Yu, J., Zheng, Y., Dong, J., Klusza, S., Deng, W.M., and Pan, D. (2010). Kibra functions as a
664 tumor suppressor protein that regulates Hippo signaling in conjunction with Merlin and Expanded.
665 Dev Cell *18*, 288-299.

666 Zanconato, F., Cordenonsi, M., and Piccolo, S. (2016). YAP/TAZ at the Roots of Cancer. Cancer
667 Cell *29*, 783-803.

668 Zeslawski, W., Beisel, H.G., Kamionka, M., Kalus, W., Engh, R.A., Huber, R., Lang, K., and Holak,
669 T.A. (2001). The interaction of insulin-like growth factor-I with the N-terminal domain of IGFBP-5.
670 EMBO J *20*, 3638-3644.

671 Zhao, B., Wei, X., Li, W., Udan, R.S., Yang, Q., Kim, J., Xie, J., Ikenoue, T., Yu, J., Li, L.*, et al.*
672 (2007). Inactivation of YAP oncoprotein by the Hippo pathway is involved in cell contact inhibition
673 and tissue growth control. Genes Dev *21*, 2747-2761.

674 Zheng, Y., Liu, B., Wang, L., Lei, H., Pulgar Prieto, K.D., and Pan, D. (2017). Homeostatic Control
675 of Hpo/MST Kinase Activity through Autophosphorylation-Dependent Recruitment of the
676 STRIPAK PP2A Phosphatase Complex. Cell Rep *21*, 3612-3623.

677 Zheng, Y., Wang, W., Liu, B., Deng, H., Uster, E., and Pan, D. (2015). Identification of
678 Happyhour/MAP4K as Alternative Hpo/Mst-like Kinases in the Hippo Kinase Cascade. Dev Cell
679 *34*, 642-655.
680

681

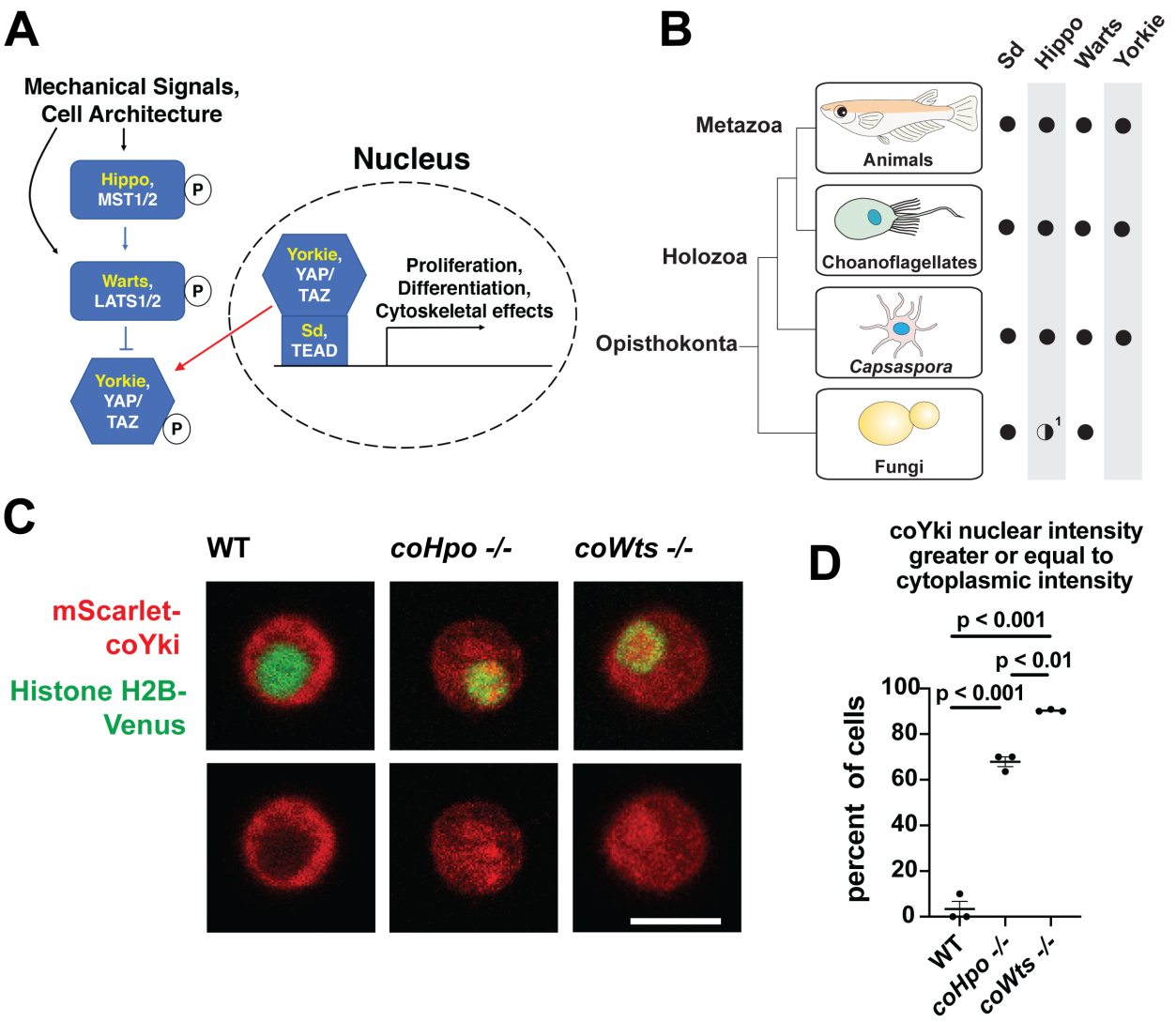


**Figure 1. The Hippo pathway kinases regulate the subcellular localization of coYki. (A)** The Hippo pathway in *Drosophila* (yellow text) and mammals (white text). Figure from (Phillips et al., 2022). **(B)** Conservation of Hippo pathway components in close unicellular relatives of animals. [1]The Hippo kinase SARAH domain is absent from putative Hippo kinase orthologs in yeasts, but is present in the early-branching fungus *Spizellomyces punctatus* and in amoebozoans such as *Dictyostelium*, indicating SARAH domain loss in some fungal lineages. Data from (Sebe-Pedros et al., 2012). **(C)** Cells were transiently transfected with the indicated constructs and imaged by confocal microscopy. Scale bar is 5 microns. **(D)** Intensity of mScarlet-coYki signal in the nucleus and cytoplasm of cells was quantified. Where p values are given, differences between conditions are significant (One-way ANOVA, Tukey's test, n = 3 with at least 10 cells measured for each independent experiment.) Values are mean ± SEM. Absence of error bars indicates that error is smaller than the plot symbol.

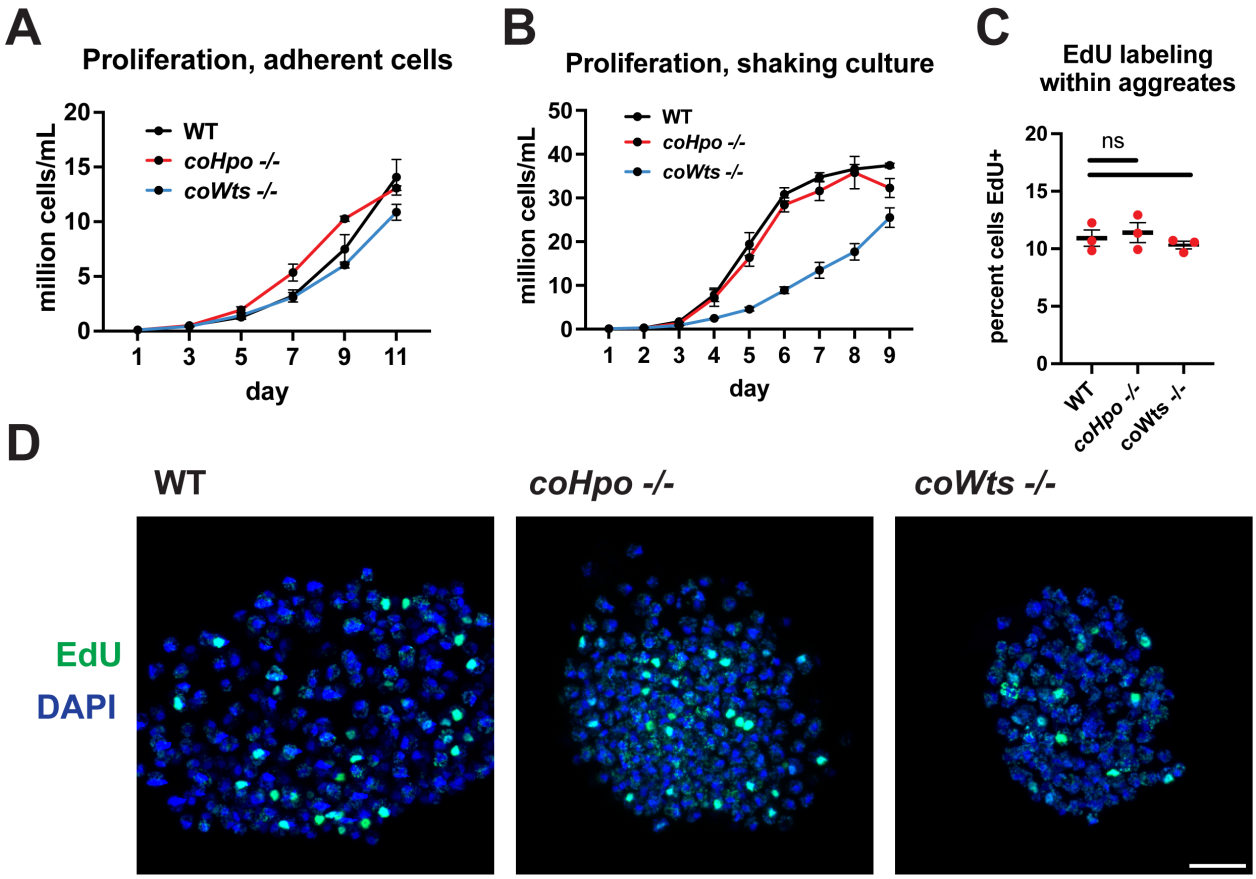


**Figure 2. The Hippo pathway kinases do not restrict cell proliferation in *Capsaspora.*** Cells were grown in adherent culture in 96-well plates **(A)** or in shaking culture **(B)** and cell density was measured daily by hemocytometer. **(C, D)** Cells were inoculated under low-adherence conditions to induce aggregate formation, and 3 days after induction aggregates were incubated with EdU for 4 hours, fixed, and processed to detect EdU labeling. Scale bar is 10 microns. Differences in EdU labeling between WT and mutants were not significant (one-way ANOVA, Dunnett's test, n = 3 with 3 aggregates measured for each independent experiment). Black bars show mean ± SEM, and red dots show values for individual aggregates.

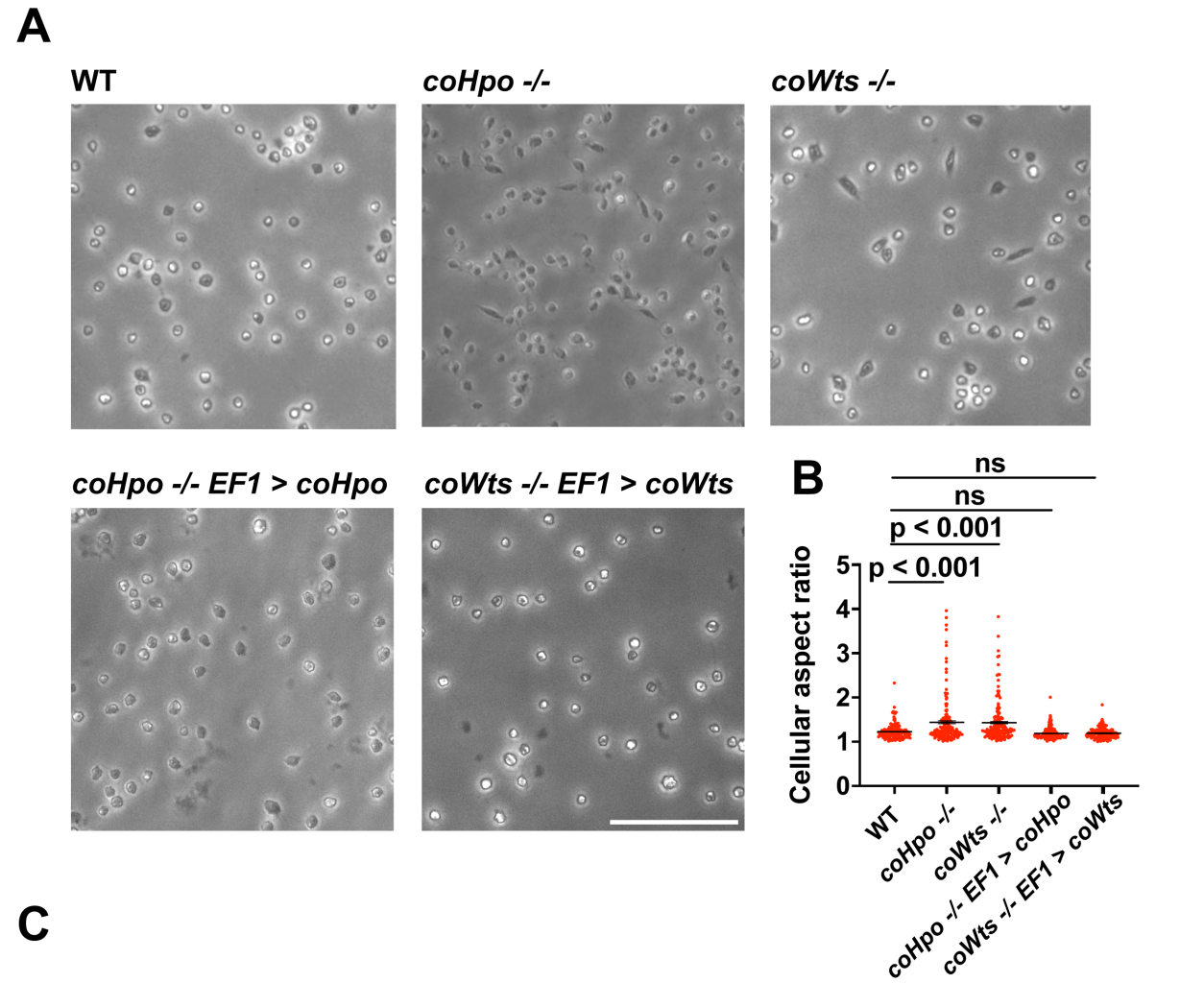
A
WT
coHpo -/-
coWts -/-
coHpo -/- EF1 > coHpo
coWts -/- EF1 > coWts
B
ns
ns
p < 0.001
p < 0.001
Cellular aspect ratio
0
1
2
3
4
5
WT
coHpo -/-
coWts -/-
coHpo -/- EF1 > coHpo
coWts -/- EF1 > coWts

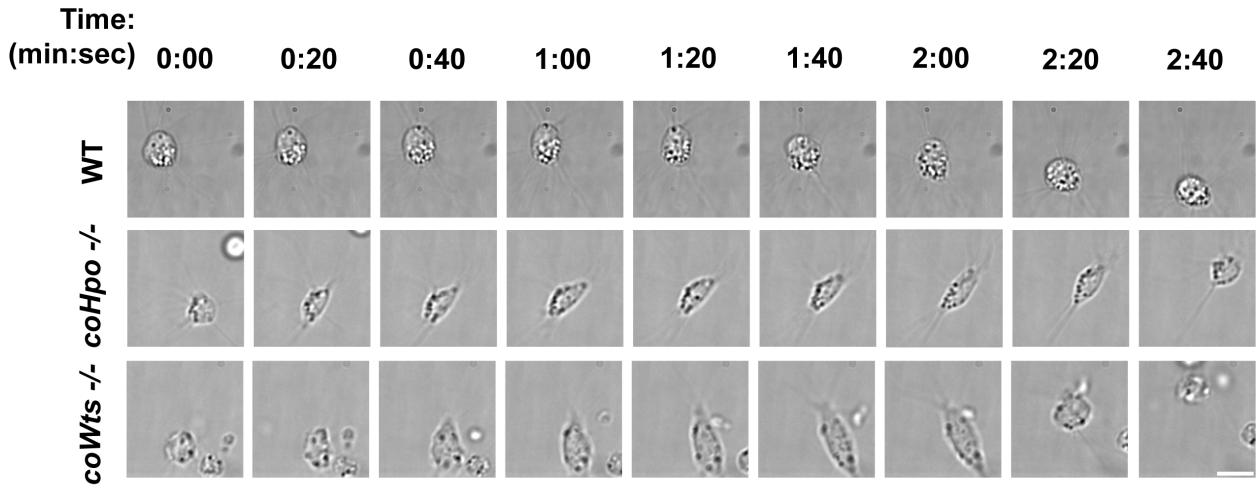
C
Time:
(min:sec)
0:00
0:20
0:40
1:00
1:20
1:40
2:00
2:20
2:40
WT
coHpo -/-
coWts -/-

708 **Figure 3. The Hippo pathway kinases regulate cell morphology and a contractile cell**
709 **behavior in *Capsaspora*. (A)** Cells were inoculated into glass-bottom chamber slides, and
710 adherent cells were imaged two days after inoculation. Scale bar is 50 microns. **(B)** The aspect
711 ratio of cells imaged as described in (A) was measured using ImageJ. The differences between
712 WT and either *coHpo -/-* or *coWts -/-* cells are significant (one-way ANOVA, Dunnett's test, n = 3
713 with 50 cells measured for each independent experiment). Black bars show mean ± SEM, and
714 red dots show values for 150 individual cells. **(C)** Cells were prepared as described in (A) and
715 imaged by time lapse microscopy. Scale bar is 10 microns.
716
717

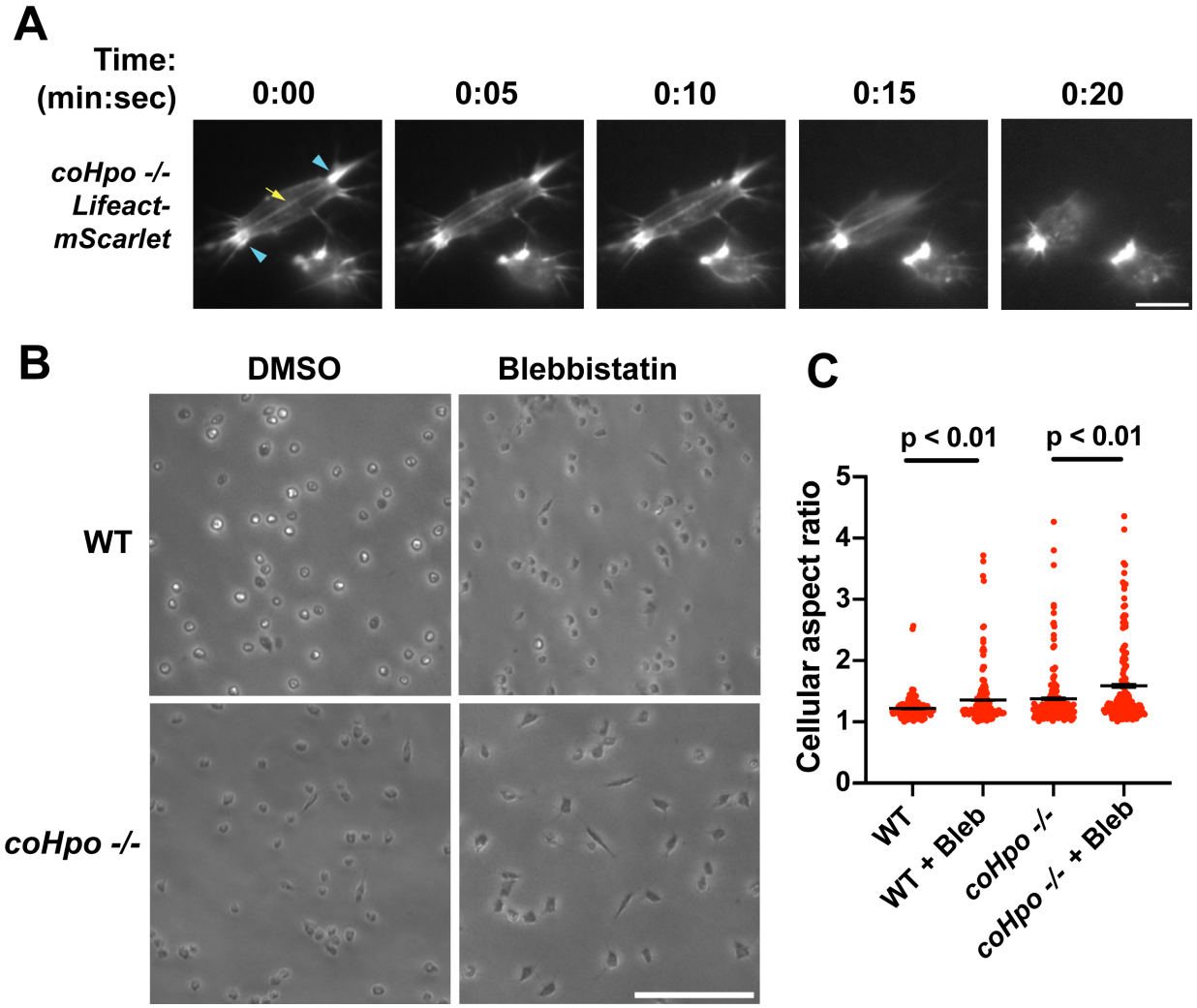


**Figure 4. Characterization of actomyosin in contractile *Capsaspora* cells. (A)** Cells were inoculated on glass-bottom chamber slides, and at 2 days after inoculation adherent cells were imaged by time-lapse epifluorescence microscopy. Blue arrowheads indicate ventral F-actin-enriched foci, and yellow arrow indicates the F-actin fiber that connects the foci. Scale bar is 10 microns. **(B)** Cells were inoculated on glass-bottom chamber slides. Two days after inoculation, DMSO or Blebbistatin at a concentration of 1 μM was added to cells. Cells were the imaged 24 hours after addition of blebbistatin. **(C)** The aspect ratio of cells prepared as in (B) was measured using ImageJ. For both WT and *coHpo -/-* cells, the difference between DMSO and blebbistatin treatment measurements are significant (t-test, n = 3 with 50 cells measured for each independent experiment). Black bars indicate mean ± SEM, and red dots indicate measurements for 150 individual cells for each condition. Absence of error bars indicates that error is smaller than the plot symbol.

732

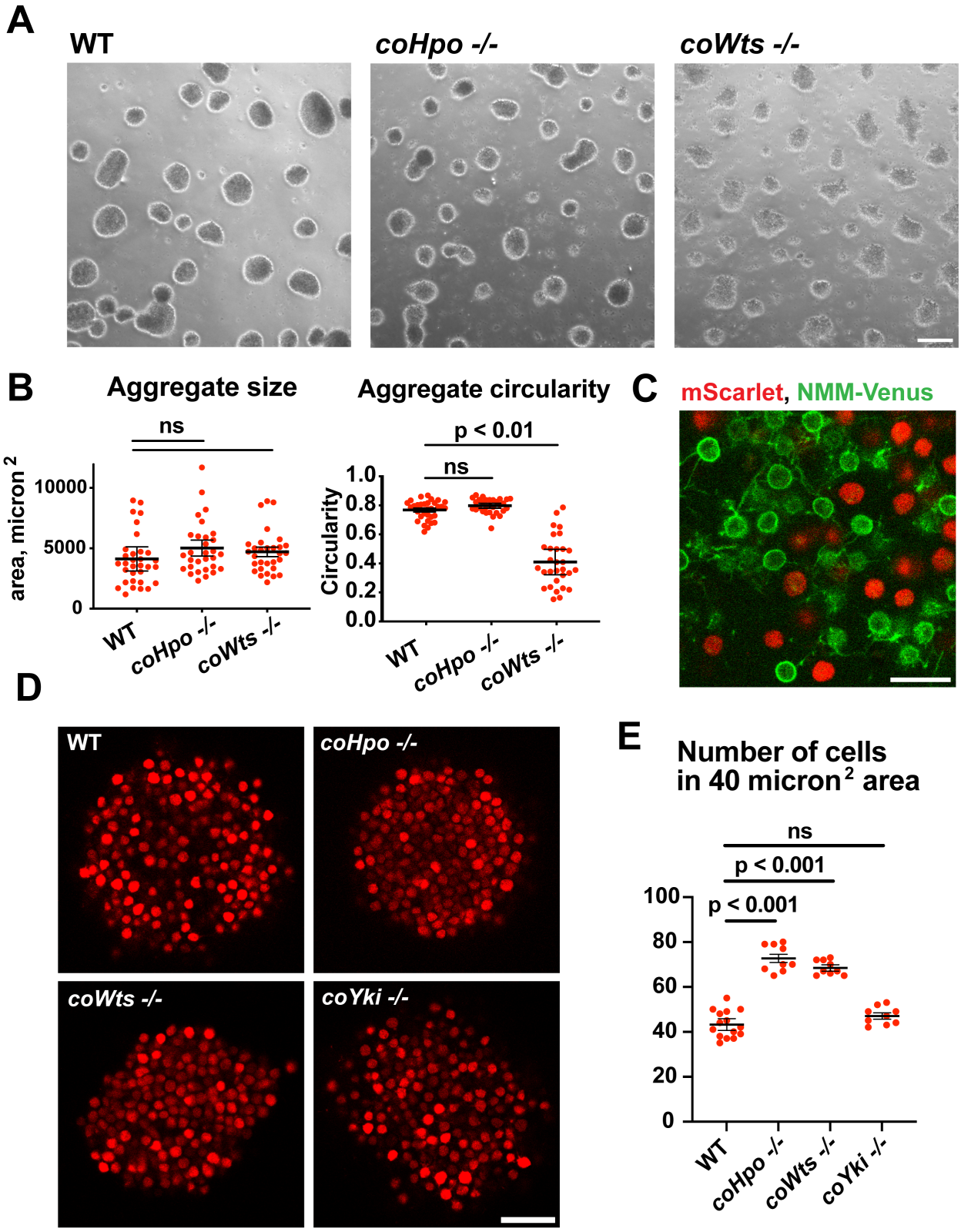
A
WT
coHpo -/-
coWts -/-
B
Aggregate size
ns
area, micron 2
10000
5000
0
WT
coHpo -/-
coWts -/-
Aggregate circularity
p < 0.01
ns
Circularity
1.0
0.8
0.6
0.4
0.2
0.0
WT
coHpo -/-
coWts -/-
C
mScarlet, NMM-Venus
D
WT
coHpo -/-
coWts -/-
coYki -/-
E
Number of cells
in 40 micron 2 area
ns
p < 0.001
p < 0.001
100
80
60
40
20
0
WT
coHpo -/-
coWts -/-
coYki -/-

733

734 **Figure 5. The Hippo pathway kinases regulate the density of cell packing in *Capsaspora***
735 **aggregates. (A)** Aggregates were induced by inoculating cells in low-adherence conditions, and
736 aggregates were imaged at 5 days after inoculation. Scale bar is 100 microns. **(B)** the size and
737 circularity of aggregates imaged as in (A) was measured using ImageJ. Black bars indicate mean
738 ± SEM (n = 3 with 10 aggregates measured for each independent experiment), and red dots
739 indicate values for 30 individual aggregates. For aggregate circularity, the difference between WT
740 and *coWts -/-* aggregates is significant (one-way ANOVA, Dunnett's test.) **(C)** Cells expressing
741 either mScarlet or N-myristoylation motif (NMM)-Venus, a marker of the plasma membrane which
742 allows visualization of filopodia, were mixed 1:1 and inoculated into low-adherence conditions to
743 induce aggregation. After 5 days, aggregates were imaged by confocal microscopy. Scale bar is
744 10 microns. **(D)** Clonal populations of cells of the indicated genotype stably expressing mScarlet
745 were inoculated into low-adherence conditions, and cell aggregates were imaged 5 days after
746 inoculation by confocal microscopy. Scale bar is 20 microns. **(E)** The number of cells within a 40
747 micron$^2$ area from aggregate optical sections imaged as in (D) was measured. Black bars indicate
748 mean ± SEM (n = 3 with 3 aggregates measured for each independent experiment), and red dots
749 indicate values for 9 individual aggregates for each condition. The difference between WT and
750 either *coHpo -/-* or *coWts -/-* cells is significant (one-way ANOVA, Dunnett's test.)
751
752

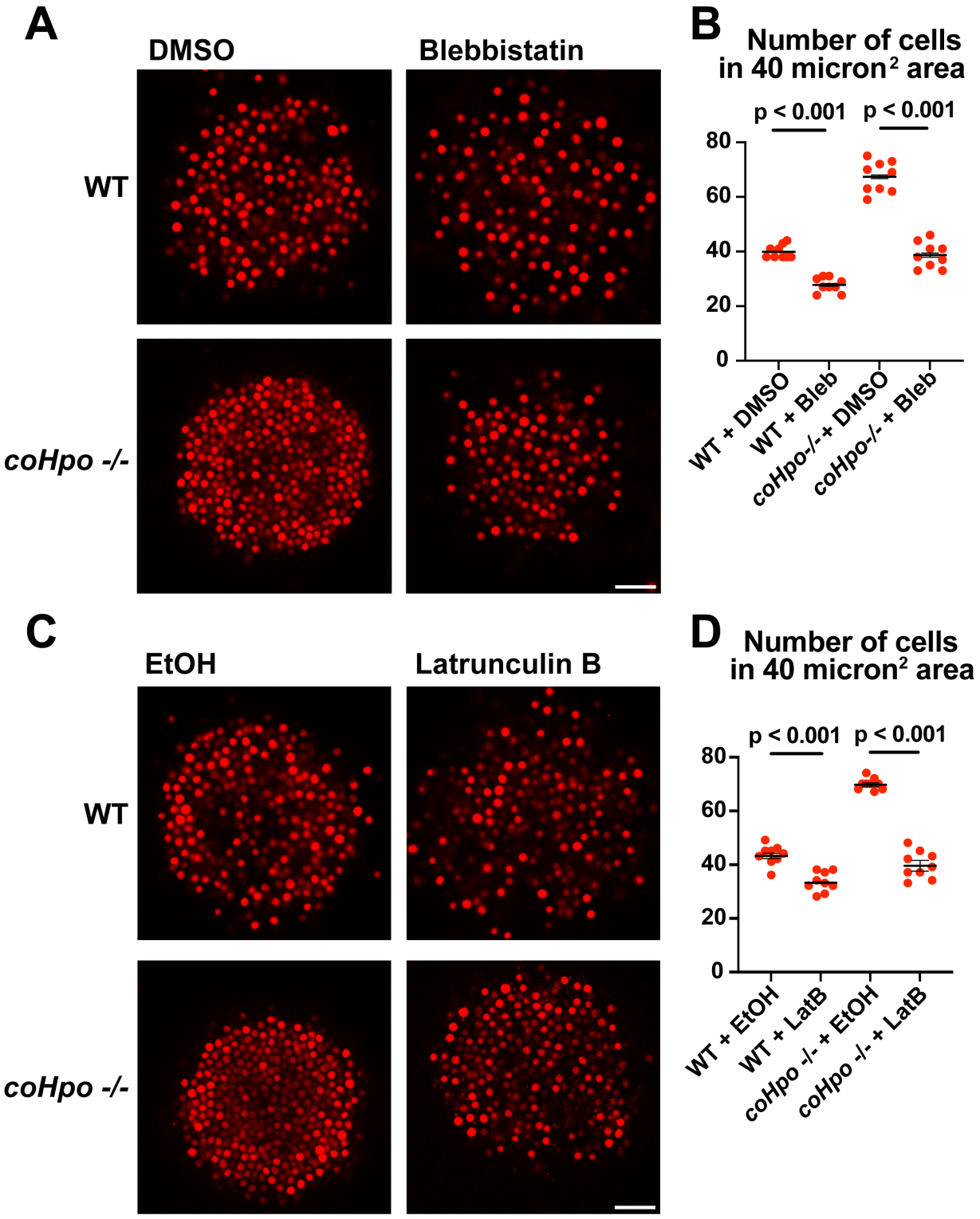


753

754

755 **Figure 6. Perturbation of the actomyosin network affects cell packing in multicellular**

756 ***Capsaspora* aggregates. (A)** Aggregates were treated with 20 μM blebbistatin or DMSO as a

757 vehicle control for 20 minutes and then imaged by confocal microscopy. Scale bar is 20 microns.
758 **(B)** Cells per area were quantified from images obtained as in (A). Black bars indicate means ±
759 SEM (n = 3 with 3 aggregates measured for each independent experiment), and red dots indicate
760 values for 9 individual aggregates for each condition. Absence of error bars indicates that error is
761 smaller than the plot symbol. For both WT and *coHpo -/-* aggregates, the difference between
762 DMSO and blebbistatin treatment is significant (t-test). **(C)** Aggregates were treated with 5 μg/ml
763 Latrunculin B or ethanol as a vehicle control for 1 hour and then imaged by confocal microscopy.
764 Scale bar is 20 microns. **(D)** Cells per area were quantified from images obtained as in (C). For
765 both WT and *coHpo -/-* aggregates, the difference between ethanol and Latrunculin B treatment
766 is significant (n = 3, t-test.)
767
768

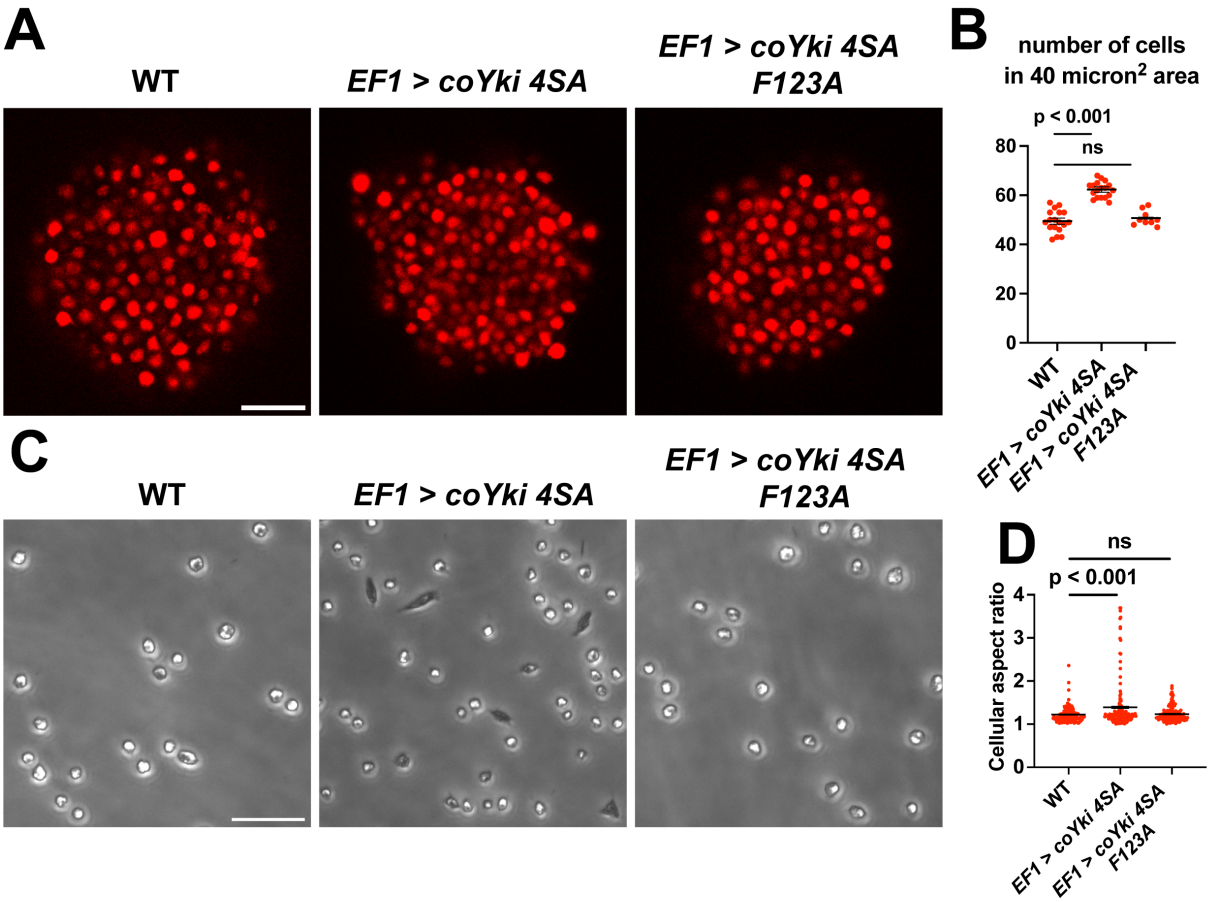


769

770 **Figure 7. Expression of a constitutively active form of coYki phenocopies loss of *coHpo***
771 **or *coWts* in *Capsaspora*. (A)** Aggregates were imaged 5 days after inoculation. Scale bar is 20
772 microns. **(B)** The number of cells within a 40 micron$^2$ area within an aggregate was measured.
773 Black bars indicate mean ± SEM (n = 3 with 3 aggregates measured for each independent
774 experiment), and red dots indicate values for 9 individual aggregates for each condition. The
775 difference between WT and *EF1 > coYki 4SA* is significant (one-way ANOVA, Dunnett's test). **(C)**
776 Cells were inoculated into glass-bottom chamber slides and imaged 2 days after inoculation.
777 Scale bar is 25 microns. **(D)** The aspect ratio of cells imaged as in (C) was measured using
778 ImageJ. Black bars show mean ± SEM (n = 3 with 40 cells measured for each independent
779 experiment), and red dots show values for 150 individual cells. The difference between WT and
780 *EF1 > coYki 4SA* is significant (one-way ANOVA, Dunnett's test ).

781

782

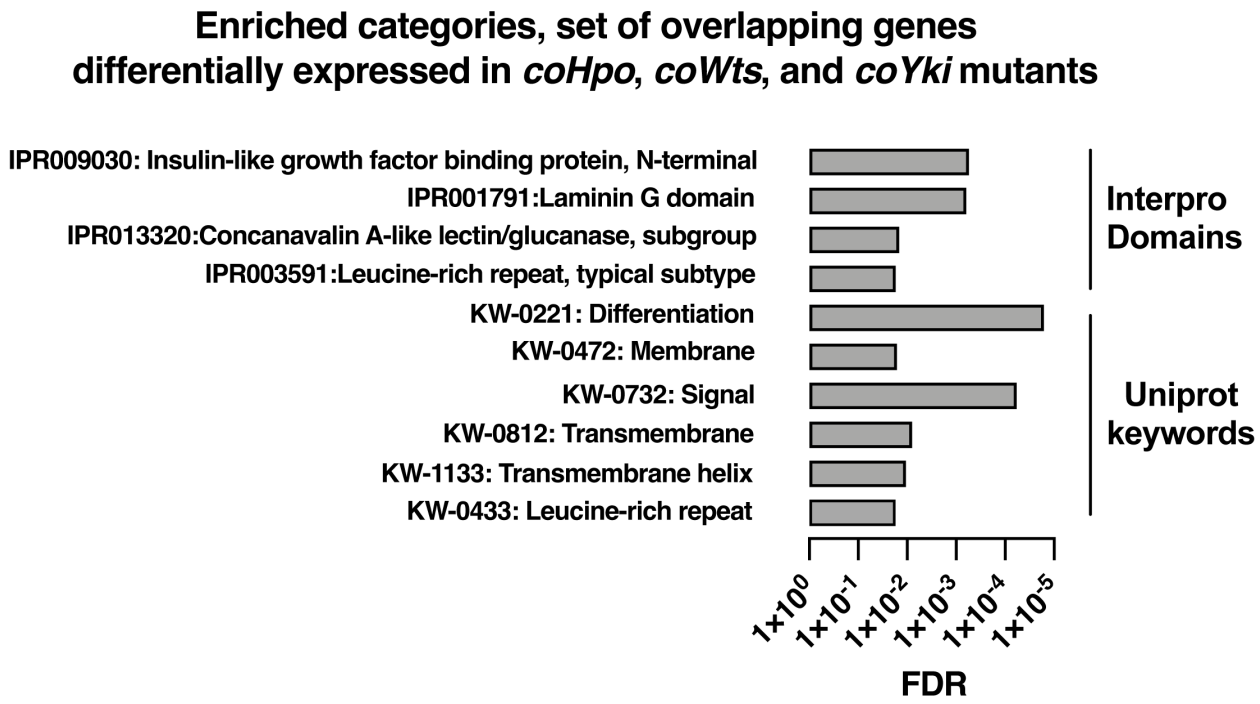


783

784

785 **Figure 8. Enrichment analysis of the overlapping set of genes differentially expressed in**
786 ***coHpo*, *coWts*, and *coYki* mutant cells.** Categories with FDR < 0.05 are shown. Interpro or
787 Uniprot accession numbers are given for each enriched category. FDR: false discovery rate.

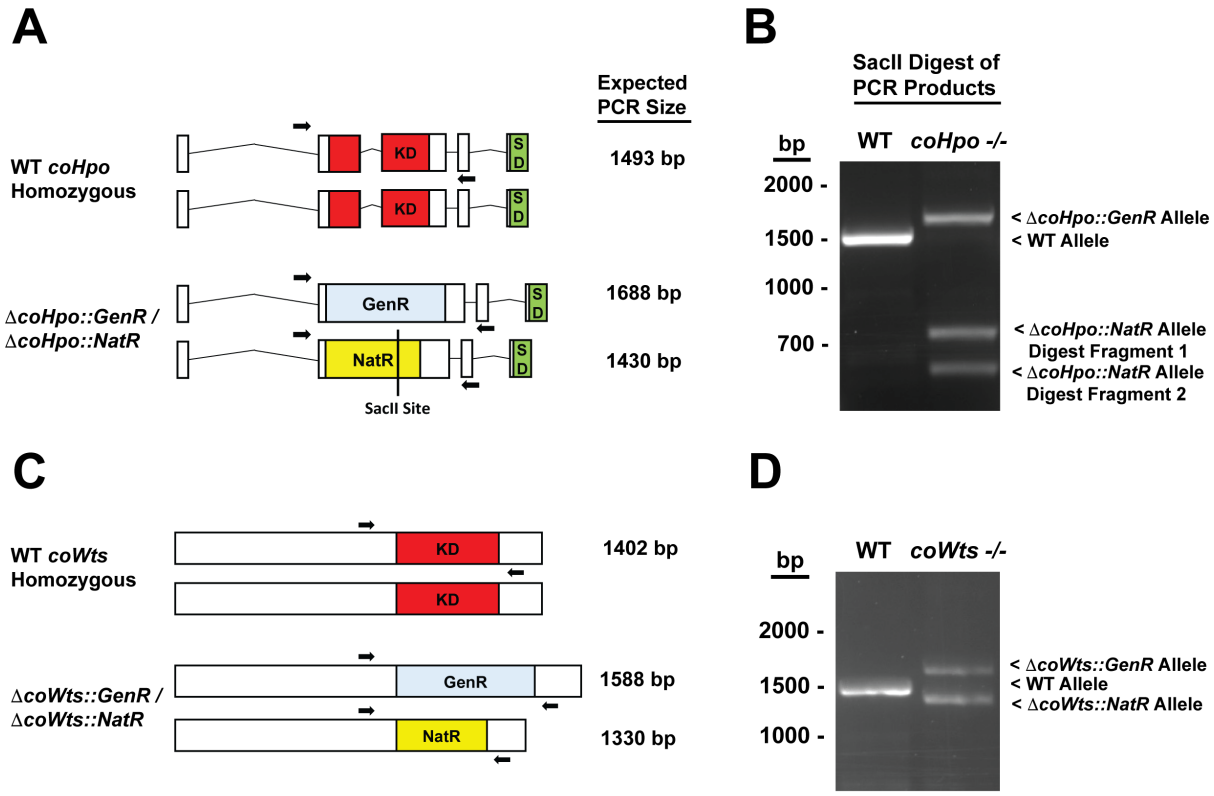


**Figure 1- figure supplement 1. Knockout of *coHpo and coWts*. (A)** A diagram of the *coHpo* genomic loci in WT or a putative *coHpo -/-* knockout line is shown. "KD" indicates kinase domain, "SD" indicates SARAH domain, "GenR" indicates a geneticin resistance cassette, and "NatR" indicates a nourseothricin resistance cassette. Arrows indicate a pair of primers used in PCR reactions. The same primer pair were used in all PCRs shown. Expected PCR product sizes for different alleles are given. A SacII site present only within the allele containing the NatR cassette is shown. **(B)** PCR products from WT and *coHpo -/-* cells using primers shown in (A). Because the product sizes for the WT and *ΔcoHpo::NatR* alleles are close in size, we digested PCR products with SacII, which uniquely cuts the *ΔcoHpo::NatR* allele. The *coHpo -/-* cell line shows the expected products for a homozygous knockout. Sequencing of PCR products confirmed the identity of the WT, *ΔcoHpo::GenR*, and *ΔcoHpo::NatR* alleles. **(C)** A diagram of the *coWts* genomic loci in WT or a putative *coWts -/-* knockout line is shown. "KD" indicates kinase domain, "GenR" indicates a geneticin resistance cassette, and "NatR" indicates a nourseothricin resistance cassette. Arrows indicate a pair of primers used in PCR reactions. The same primer pair were used in all PCRs shown. **(D)** PCR products from WT and *coHpo -/-* cells using primers shown in (C). The *coWts -/-* cell line shows the expected products for a homozygous knockout.

806 Sequencing of PCR products confirmed the identity of the WT, *⊿coWts::GenR*, and *⊿coWts::NatR*
807 alleles.
808
809

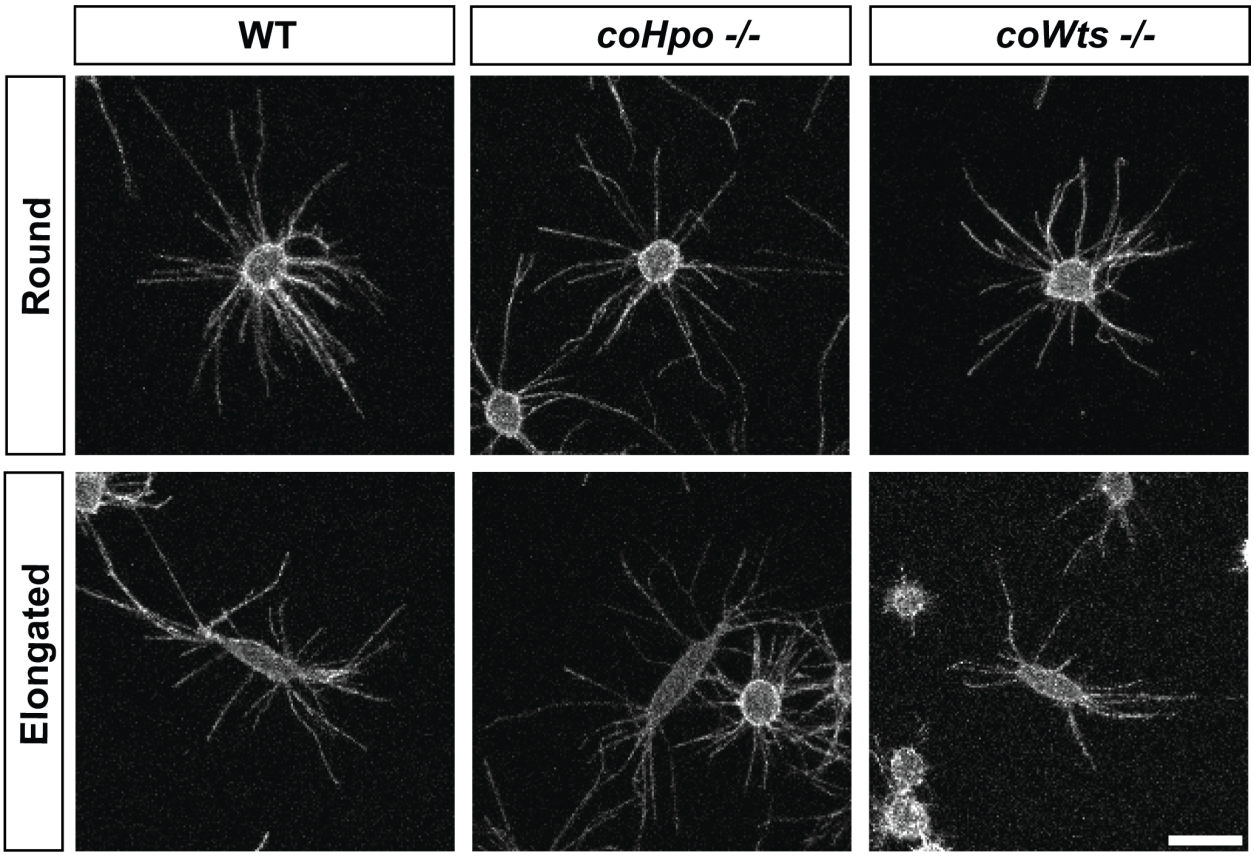


**Figure 3- figure supplement 1. Filopodia are enriched at the poles of elongated cells.** Adherent cells stably expressing NMM-Venus, a plasma membrane marker which allows for visualization of filopodia, were imaged live by confocal microscopy. Scale bar is 10 microns.

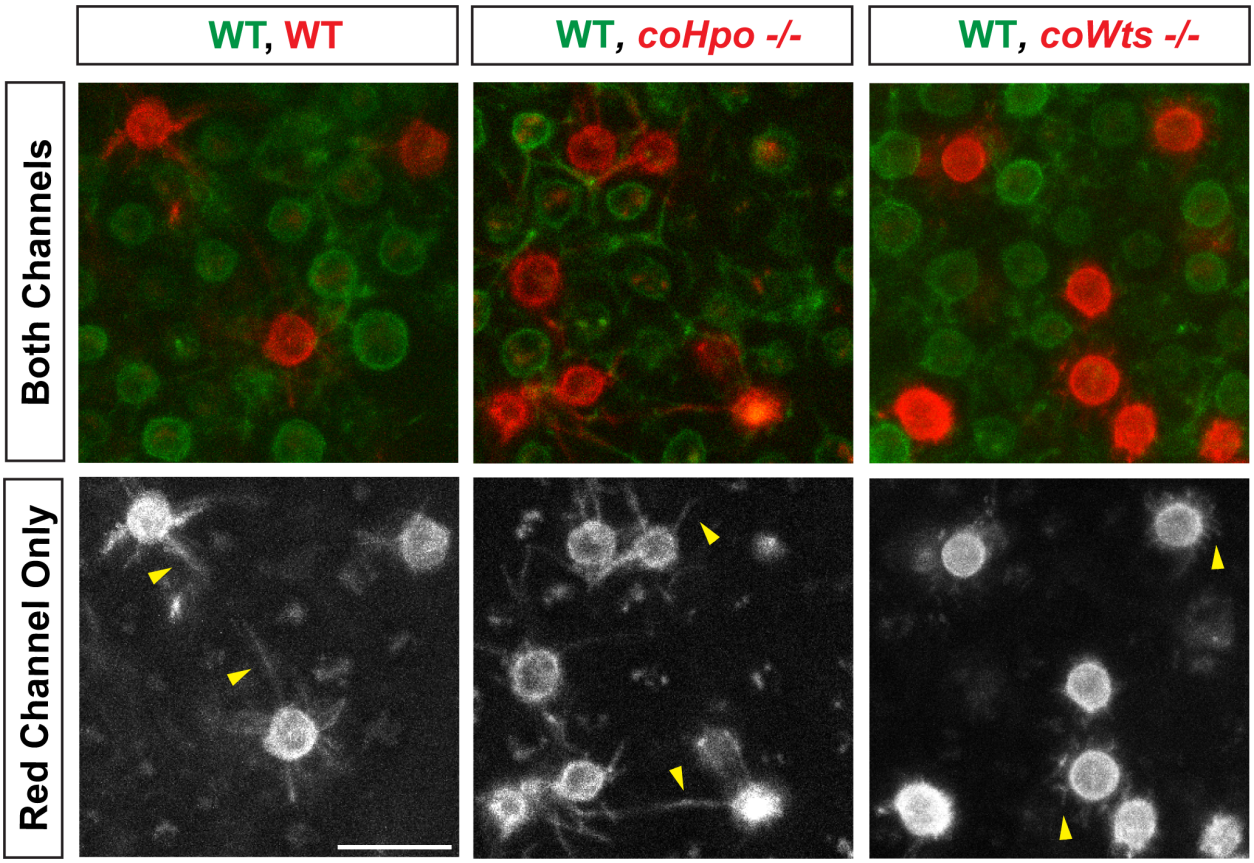


**Figure 5- figure supplement 1. *coWts* -/- cells within multicellular aggregates show altered filopodial morphology and reduced filopodial length.** WT cells stably expressing NMM-Venus, which allows visualization of filopodia, were mixed with WT, *coHpo* -/-, or *coWts* -/- cells stably expressing NMM-mScarlet at a 9:1 cell ratio and were inoculated into low-adherence wells to induce aggregate formation. Cells within aggregates were then imaged three days after aggregate induction. Yellow arrowheads indicate examples of filopodia. Scale bar is 10 microns.

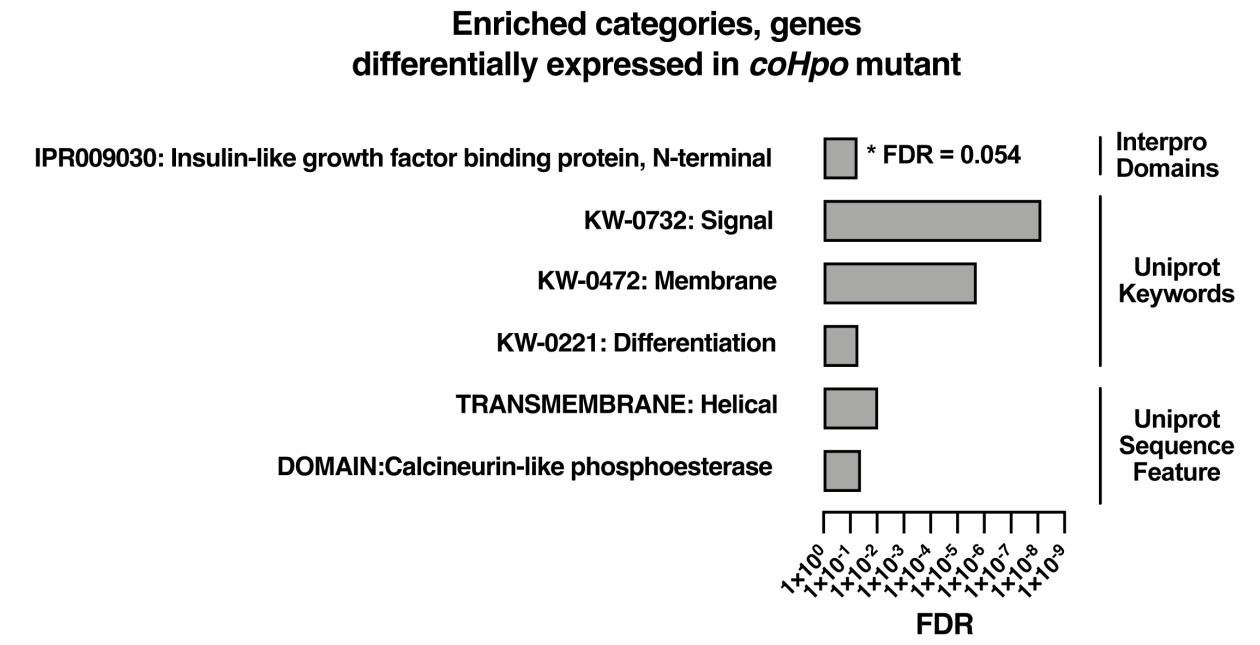


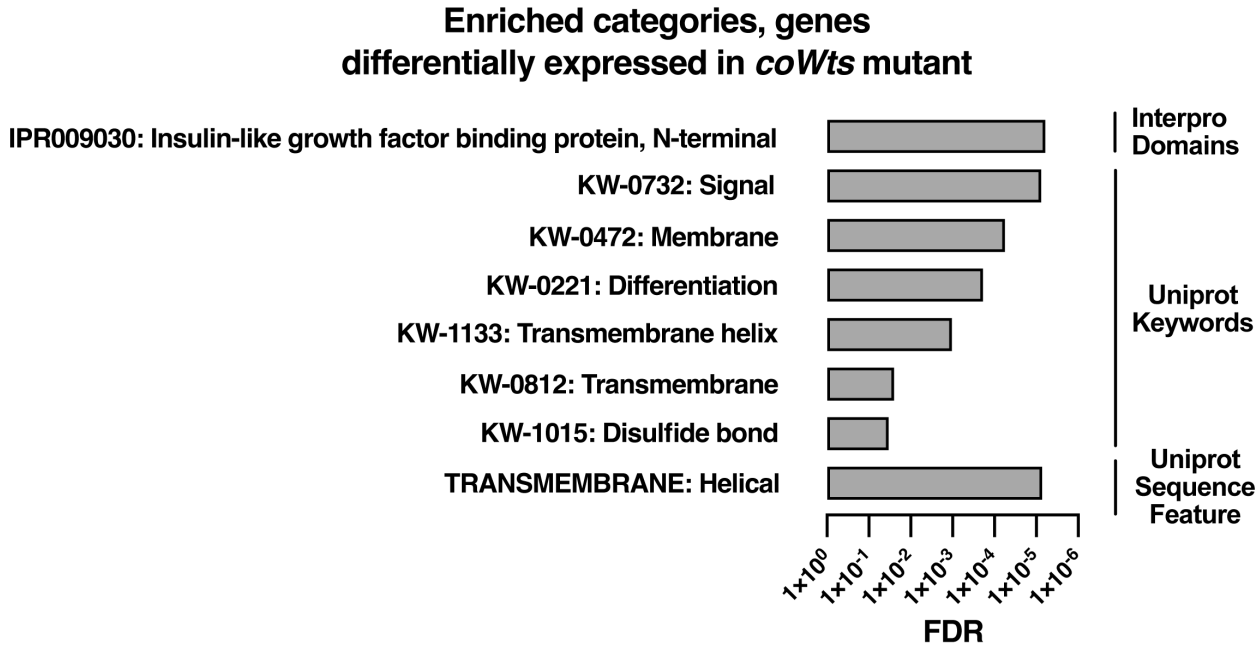


**Figure 8- figure supplement 1. Enrichment analysis for genes differentially expressed in coHpo or coWts mutant cells.** Categories with FDR < 0.05 are shown, except where FDR is indicated. Interpro or Uniprot accession numbers are given for enriched categories where appropriate. FDR: false discovery rate.

833 **Video S1. Time-lapse microscopy of adherent WT *Capsaspora* cells.** This video serves as a
834 control for Videos S2 and S3.
835
836 **Video S2. Time-lapse microscopy of adherent *coHpo -/-* cells.**
837
838 **Video S3. Time-lapse microscopy of adherent *coWts -/-* cells.**
839
840 **Video S4. Time-lapse confocal microscopy of adherent WT cells expressing Lifeact-**
841 **mScarlet.** This video serves as a control for Video S5.
842
843 **Video S5. Time-lapse confocal microscopy of adherent *coHpo -/-* cells expressing Lifeact-**
844 **mScarlet.**
845

846 **Supplementary File 1. Genes with actin binding functional annotation showing**
847 **differential expression in *coYki* mutant cells and also exhibiting differential expression in**
848 ***coHpo* and/or *coWts* mutant cells**
849
850 **Supplementary File 2. Lists of genes differentially expressed in *coHpo* mutant cells,**
851 **coWts mutant cells, and the overlapping set of genes differentially expressed in *coHpo*,**
852 ***coWts*, and *coYki* mutant cells.**
853
854 **Supplementary File 3. Sequences of synthesized gene fragments used in this study**
855
856

857 **Figure 1-supplement 2-source data 1. Unedited gel image used to generate panel B.**
858
859 **Figure 1-supplement 2-source data 2. Uncropped annotated gel image used to generate**
860 **panel B.**
861
862 **Figure 1-supplement 2-source data 3. Unedited gel image used to generate panel D.**
863
864 **Figure 1-supplement 2-source data 4. Uncropped annotated gel image used to generate**
865 **panel D.**
866
867